Activation mechanism of ATP-sensitive K^+ channels explored with real-time nucleotide binding

Michael C. Puljung, Natascia Vedovato, Samuel Usher, Frances M. Ashcroft*

Department of Physiology, Anatomy & Genetics, University of Oxford, Oxford UK OX1 3PT

*Address correspondence to Frances Ashcroft, frances.ashcroft@dpag.ox.ac.uk

Author contributions: MCP and FMA designed the experiments. MCP, NV, and SU performed the experiments. MCP and FMA wrote the manuscript.

Keywords:

Ion channel, allostery, binding, gating, diabetes, ligand, metabolism

Abstract

The response of ATP-sensitive K^+ channels (K_{ATP}) to cellular metabolism is coordinated by three classes of nucleotide binding site (NBS). We used a novel approach involving labeling of intact channels in a native, membrane environment with a non-canonical fluorescent amino acid and measurement (using FRET with fluorescent nucleotides) of steady-state and time-resolved nucleotide binding to dissect the role of NBS2 of the accessory SUR1 subunit of K_{ATP} in channel gating. Binding to NBS2 was Mg^{2+}-independent, but Mg was required to trigger a conformational change in SUR1. Mutation of a lysine (K1384A) in NBS2 that coordinates bound nucleotides increased the EC_{50} for trinitrophenyl-ADP binding to NBS2, but only in the presence of Mg^{2+}, suggesting that this mutation disrupts the ligand-induced conformational change. Comparison of nucleotide-binding with ionic currents suggests a model in which each nucleotide binding event to NBS2 of SUR1 is independent and promotes K_{ATP} activation by the same amount.

Introduction

ATP-sensitive K^+ channel (K_{ATP}) closure initiates the electrical response of pancreatic β-cells to metabolic changes induced by increased extracellular glucose[1,2]. K_{ATP}'s metabolic sensitivity is accomplished through the coordinated activity of three classes of intracellular adenine nucleotide binding site (NBS), one inhibitory and two stimulatory. Despite the recent publication of several cryo-EM structures of K_{ATP} showing these NBSs at near atomic resolution[3-6], the detailed mechanism by which energetic contributions from nucleotide binding to each site sum to affect channel gating remains obscure.

K_{ATP} is formed by four inward-rectifier K^+ channel subunits (Kir6.2 in β-cells)[7,8], each associated with a modulatory sulfonylurea receptor (SUR1 in β-cells)[9,10] (Fig. 1a). The inhibitory NBS of K_{ATP} is located on Kir6.2[11] and clearly resolved in several of the cryo-EM structures[3-6]. Like other ATP-binding cassette (ABC) proteins, SUR1 has two cytoplasmic nucleotide binding domains (NBDs), which associate to form two NBSs at the dimer interface (Fig. 1a,c)[3]. These mediate K_{ATP} activation by Mg-nucleotides[11,12]. SUR1 also confers inhibition by antidiabetic sulfonylureas (SUs) and activation by K_{ATP}-specific K^+ channel openers (KCOs)[11-14].

Gating of K_{ATP} is a complex function of the intrinsic opening and closing of the channel pore and the converging influences of the excitatory and inhibitory NBSs. Mutations that directly disrupt the NBSs or their ability to transduce nucleotide occupancy to the pore result in diseases of insulin secretion[2,15]. It is crucial to our understanding of K_{ATP} to be able to independently measure (i) the occupancy of each NBS in real time, (ii) the effect each NBS has on K_{ATP} conformation, and (iii) how binding to each NBS affects channel open probability (P_{open}). Electrophysiology, radioligand binding, and ATPase assays have provided rich mechanistic insight into K_{ATP} gating. However, the ultimate readout of such studies is a function of nucleotide binding to all three NBSs as well as the conformational equilibria affected by binding. Photoaffinity labeling studies enable binding to each NBS to be separated, and some determination of their affinity and specificity, but require partially purified proteins, long incubation times, and involve irreversible covalent labeling[16].

An ideal method to separate the nucleotide interactions at each class of site on K_{ATP} would have high spatial (specific for a single NBS) and temporal resolution, would require only small amounts of protein, could be used in a native environment (i.e. the cell or plasma membrane), and would operate under conditions compatible with electrophysiological experiments. We have developed a novel approach for studying ligand binding that fits these criteria. K_{ATP} was labeled with the fluorescent non-canonical amino acid L-3-(6-acetylnaphthalen-2-ylamino)-2-aminopropionic acid (ANAP)[17] and binding of fluorescent, trinitrophenyl (TNP) nucleotide derivatives was measured using FRET. This enabled us to parse the individual contribution of NBS2 to nucleotide binding/channel gating and has provided insight into the mechanism by which Mg-nucleotides affect the conformation of SUR1, and the effect this conformational change has on P_{open}.

Results

Nucleotide binding to NBS2. Binding of nucleotides to NBS2 is believed to stimulate K_{ATP} activation[12,18]. ANAP was introduced at position Y1353 (Y1353*) of NBS2 using a transfectable amber codon suppression system (Fig. 1b,c)[17] and fluorescence emission spectra were acquired from "unroofed" membrane fragments expressing SUR1-Y1353*/Kir6.2 (Fig. 1d,e; Fig. S1a)[19-21]. In the nucleotide-bound structures of K_{ATP}, the aromatic ring of Y1353 forms a π-stacking interaction with the adenine ring of ADP[3,6].

To probe nucleotide binding to K_{ATP}, we measured FRET between SUR1-Y1353*/Kir6.2 and fluorescent TNP-nucleotides (Fig. 1b,d,e). The absorbance spectra of TNP nucleotides overlap with the emission spectrum of SUR1-Y1353* (Fig. S2a), making them suitable FRET partners. Fig. S2b shows the calculated distance dependence of FRET between SUR1-Y1353* and TNP-nucleotides. This steep distance dependence provides the spatial resolution necessary to discriminate between nucleotides bound directly at NBS2 (FRET efficiency close to 100%) or at other sites.

TNP-nucleotides have been used previously to probe nucleotide binding to several ABC proteins including NBD1 of SUR2A, as well as the cytoplasmic domain of Kir6.2[22-24]. Fig. 2c,d shows that MgTNP-ADP was able to activate K_{ATP} formed by wild-type SUR1 with a mutated Kir6.2 (Kir6.2-G334D) in inside-out patches (Table 2). G334D disrupts inhibitory nucleotide binding to Kir6.2[25], allowing activation to be measured in isolation[26].

FRET between SUR1-Y1353*/Kir6.2 and bound TNP-ADP produced a concentration-dependent decrease (quenching) of the donor ANAP peak at 470 nm and a concomitant increase in the TNP-ADP fluorescence at ~565 nm (Fig. 1d,e). We quantified nucleotide binding using the decrease in ANAP fluorescence, as this signal was specific to K_{ATP} (Fig. S1b,c) and we observed non-specific association of TNP-nucleotides in sham-transfected membranes at high concentrations (Fig. S2e). No change in fluorescence was observed when saturating concentrations of MgATP or MgADP were applied to SUR1-Y1353*/Kir6.2 channels (Fig. S2f), indicating that quenching of the ANAP signal results from FRET and not an allosteric change in the environment surrounding 1353* caused by nucleotide binding.

Fig. 1f shows concentration-response relationships for binding of MgTNP-ATP and MgTNP-ADP to SUR1-Y1353*/Kir6.2 channels. Both nucleotides quenched ANAP completely, consistent with direct binding of TNP-nucleotides at NBS2. MgTNP-ADP bound with ~7-fold lower EC_{50} than MgTNP-ATP (Table 1), consistent with the lower EC_{50} for activation of SUR1/Kir6.2-G334D channels by MgADP vs. MgATP (7.7 μM vs. 112 μM)[26].

Quite unexpectedly, we observed binding of both TNP-ATP and TNP-ADP to NBS2 in the *absence* of Mg^{+}, i.e. in 1 mM EDTA (Fig. 1g). Both nucleotides bound with similar affinities in the absence of Mg^{2+} (Table 1), but neither fully quenched SUR1-Y1353*/Kir6.2 fluorescence (Fig. 1g). Although quenching was not 100%, the amount of FRET obtained in the absence of Mg^{2+} is still consistent with nucleotides binding at NBS2. The difference in FRET efficiency at saturating nucleotide concentrations in the presence and absence of Mg^{2+} may reflect a change in orientation between the donor and acceptor, as the NBDs are expected to change conformation in the presence of Mg^{2+}[3,4].

Despite the relatively close proximity of NBS1 to Y1353* (39 Å to TNP-ATP aligned at NBS1, Fig. 1c), the FRET we observes was primarily the result of quenching by TNP-ATP/ADP bound at NBS2. When nucleotides are bound directly to NBS2, FRET efficiency is very high and any nucleotide binding at NBS1 would have little or no effect on our measurements[27]. Nucleotides at NBS1 would only contribute to the observed FRET signal if NBS2 were unoccupied. However, with no nucleotide bound to NBS2, the NBDs would not dimerize and 1353* would be ~56 Å away from TNP-nucleotides bound to NBS1 (based on PDB 6BAA)[4]. At this distance, the predicted FRET efficiency is <20% (Fig. S2b), much less that the FRET efficiencies we observed for TNP nucleotide quenching $\pm Mg^{2+}$ (Fig. 1f,g; Table 1).

In the Mg-nucleotide-bound "quatrefoil" structure of K_{ATP}, the inhibitory NBS of Kir6.2 is within ~33 Å of Y1353 (Fig. S3a)[3]. To eliminate a possible contribution of nucleotide bound at Kir6.2 to our measured FRET signal, we measured binding of MgTNP-ADP to SUR1-Y1353* co-expressed with Kir6.2-G334D (Fig. S3b). The EC_{50} was very similar to that measured with SUR1-Y1353*/Kir6.2 (Table 1), suggesting that either the NBS on Kir6.2 was too distant for FRET with Y1353*, or that appreciable binding to Kir6.2 did not occur at concentrations at which NBS2 was unoccupied.

Mg^{2+} locks nucleotides at NBS2. If nucleotides can bind NBS2 in the absence of Mg^{2+}, why is K_{ATP} only activated in the presence of Mg^{2+}? The simplest explanation is that binding to NBS2 is Mg^{2+}-independent, but Mg^{2+} is required to support the conformational change that promotes channel activation. Presumably, this conformational change involves NBD dimerization, as observed in the structures of K_{ATP}[3,6]. Because nucleotide dissociation would require opening of the NBD dimer, it is expected to slow the nucleotide off rate. We therefore measured the time course of nucleotide dissociation from SUR1-Y1353*/Kir6.2 in the presence and absence of Mg^{2+}.

In the absence of Mg^{2+}, TNP-ADP dissociated very rapidly from SUR1-Y1353*/Kir6.2 (Fig. 2a,e; Table 3). Dissociation of TNP-ADP was greatly slowed by the presence of Mg^{2+} ($p = 0.001$). Similar, but less dramatic results were obtained with TNP-ATP (Fig. 2b,e; $p = 0.0001$; Table 3). Whereas the time courses of dissociation of TNP-ADP $\pm Mg^{2+}$ and TNP-ATP in the presence of Mg^{2+} were well described

by single exponential decays, the dissociation of TNP-ATP in the absence of Mg^{2+} appeared biexponential.

Our data are consistent with an activation model for K_{ATP} in which the NBDs of SUR1 dimerize in the presence of Mg^{2+}, preventing rapid nucleotide dissociation. However, it is formally possible that Mg^{2+} could directly stabilize nucleotide binding without any conformational change in the NBDs. In a two-state binding equilibrium for TNP-nucleotides and SUR1 (SCHEME 1),

$$\text{TNP-nucleotide} + \text{SUR1} \underset{k_{off}}{\overset{k_{on}}{\rightleftharpoons}} \text{TNP-nucleotide}\cdot\text{SUR1} \qquad \text{SCHEME 1}$$

the dissociation constant, K_d, is equal to k_{off}/k_{on}. Therefore, any effect on k_{off} (e.g. via a direct stabilization of nucleotide binding by Mg^{2+}) would affect K_d proportionately. In our experiments, the off-rate for TNP-ADP was reduced ~5-fold in the presence of Mg^{2+}, whereas the EC_{50} for TNP-ADP was largely unaffected (Fig. S4a, Table 1,3). Mg^{2+} reduced the off-rate for TNP-ATP by a factor of 2.2, but actually increased the EC_{50} for binding by a factor of ~3 (Fig. S4b, Table 1,3). These results are not compatible with a simple equilibrium as shown in Scheme 1. A more parsimonious explanation is that, in the presence of Mg^{2+}, there is no longer a simple equilibrium for binding and unbinding and that Mg-nucleotide binding is coupled to an additional process, which we propose is the activating conformational change in SUR1 (starting with NBD dimerization).

To test this hypothesis, we examined nucleotide dissociation rates in the presence of the sulfonylurea (SU) tolbutamide (Fig. 2c,d,e, Table 3). The cryo-EM structure of Kir6.2/SUR1 in the presence of glibenclamide suggests that SUs prevent NBD dimerization[4], and electrophysiological studies further suggest that SUs prevent Mg-nucleotide induced current activation[28]. In the presence of tolbutamide, the dissociation rates for MgTNP-ADP and MgTNP-ATP were not significantly different from those measured for nucleotides in the absence of both tolbutamide and Mg^{2+} (Fig. 2e, Table 3; $p = 0.07$, for TNP-ADP, $p = 1$ for TNP-ATP). This argues that the slower off rate for TNP-ADP and TNP-ATP in the

presence of Mg^{2+} must result from NBD dimerization, not a direct stabilization of nucleotide binding by Mg^{2+}.

As further support, we tested the effect of diazoxide (a KCO) on the nucleotide dissociation rate. It has been proposed that nucleotide binding at the NBDs of SUR2A stabilizes binding of the KCO pinacidil[29]. The time course of nucleotide dissociation in the presence of diazoxide did not follow a single exponential decay, but the drug greatly reduced the dissociation rates for both MgTNP-ADP and MgTNP-ATP (Fig. 2c,d,e; Table 3). This suggests that KCOs function by stabilizing the activated (NBD-dimerized) conformation of SUR1.

The nucleotide dissociation rates measured in the presence of Mg^{2+} are slower than the deactivation rates observed for SUR1/Kir6.2-G334D currents following nucleotide washout[26]. However, it should be noted that current decay reflects a conformational change in the channel and not the rate of nucleotide dissociation, and may be affected by the presence of four SUR1 monomers per channel. Furthermore, the deactivation rates were measured for MgATP/ADP and not TNP-nucleotides. Ultimately, a direct comparison of TNP-nucleotide dissociation rates and deactivation rates will require simultaneous measurement of current and binding.

Mutation of the Walker$_A$ lysine of NBS2 affects channel conformation, not nucleotide binding. Our ability to measure nucleotide binding to SUR1 in the presence and absence of Mg^{2+} provides a framework for mechanistically separating nucleotide binding from the conformational changes that occur subsequent to binding. In the presence of Mg^{2+} the apparent nucleotide affinity is influenced by both binding and the conformational change. In the absence of Mg^{2+}, however, no conformational change is expected and the apparent affinities measured reflect true (state-independent) binding affinities. Therefore, mutations that affect the apparent nucleotide affinity in the presence and absence of Mg^{2+} can be interpreted as direct effects on ligand binding, whereas mutations that only affect the apparent nucleotide affinity in the presence of Mg^{2+} must exert their effect on binding allosterically.

We mutated the lysine residue in the $Walker_A$ motif of NBS2 to alanine (K1384A) in channels labeled with ANAP at NBS2 (SUR1-Y1353*,K2A/Kir6.2) and measured nucleotide binding with and without Mg^{2+} (Fig. 3). In other ABC proteins, and in the Mg-nucleotide-bound structure of K_{ATP}, the $Walker_A$ lysine coordinates the β- and γ-phosphates of bound nucleotides (Fig. 3a).

In the absence of Mg^{2+} we observed no significant difference in TNP-ATP and TNP-ADP binding to SUR1-Y1353*,K2A/Kir6.2 compared to SUR1-Y1353*/Kir6.2 (Fig. 3b,c; Table 1). MgTNP-ATP binding was also unaffected by the K2A mutation (Fig. 3d; Table 1). However the K2A mutation disrupted MgTNP-ADP binding (EC_{50} = 16.5 μM for K2A vs. 4.8 μM for SUR1-Y1353*, $p = 0.04$; Fig. 3e, Table 1). As we observed no change in TNP-ADP binding in the absence of Mg^{2+}, we conclude that the K2A mutation affects nucleotide binding indirectly, by reducing the ability of MgTNP-ADP to cause NBD dimerization. Consistent with this, the K2A mutation also affected the slope of the MgTNP-ADP concentration-response relationship ($p = 0.03$, Table 1), which would not be expected from a change in the intrinsic binding affinity. To confirm this result, we measured the rate of MgTNP-ADP dissociation from SUR1-Y1353*,K2A/Kir6.2 (Fig. 3f). The K2A mutation increased the off-rate for MgTNP-ADP compared to SUR1-Y1353*/Kir6.2 channels (Table 2; $p = 0.04$), implying the K2A mutant destabilized NBD dimerization. Consistent with this, previous electrophysiological studies showed that the K2A mutation reduced the maximal MgATP activation of SUR1/Kir6.2-G334D and shifted the concentration dependence of MgADP activation >20-fold to higher concentrations, such that the maximal response could not be determined[28].

Correlation of binding with gating. We next sought to correlate nucleotide binding with changes in channel activity. Despite our ability to demonstrate a Mg^{2+}- and nucleotide-dependent conformational change in SUR1-Y1353*/Kir6.2, we were unable to measure activation of SUR1-Y1353*/Kir6.2 channels by Mg-nucleotides. There are two possible explanations for this observation. The first is that SUR1-Y1353* disrupts communication between the NBD-dimerized SUR1 and Kir6.2. Inspection of the Mg-

nucleotide-bound "quatrefoil" structure[3] shows that position 1353 is adjacent to residues (e.g. R1352) at the interface between SUR1 and Kir6.2. Mutation of R1352 disrupts K_{ATP} activation[30,31].

Another possible explanation for the lack of K_{ATP} current activation is that channels containing SUR1 subunits truncated at Y1353 (i.e. no ANAP incorporated) trafficked to the plasma membrane. These channels would not be expected to support activation as they lack a complete NBS2. In fluorescence measurements, we only observe full-length SUR1-Y1353*/Kir6.2 channels as only these are labeled with ANAP (Fig. S1). However, in electrophysiological experiments there is no *a priori* way of distinguishing between currents through channels with truncated SUR1 and full-length channels with impaired activation coupling.

Anecdotally, we noticed no difference in the current magnitude from patches excised from cells expressing SUR1-Y1353^{amber}/Kir6.2 in the presence of ANAP (where full-length channels will be present) or in its absence (where all channels would be expected to be truncated). Using a surface expression assay[32], we also observed no difference in the ability of full-length and truncated SUR1-Y1353^{amber} to chaperone HA-tagged Kir6.2 to the plasma membrane (Fig S5a). We therefore sought to label an additional position near NBS2 for which only full-length, ANAP-labeled channels would support surface expression of Kir6.2. We mutated 34 different residues (amino acids 1386-1397, 1400-1408, and 1410-1423) to the amber stop codon and screened the constructs for their ability to promote surface expression of HA-Kir6.2 only in the presence of ANAP. We focused on SUR1-T1397^{amber}, as this mutation strongly increased the surface expression of HA-Kir6.2 in the presence of ANAP (Fig. S5a; $p = 0.005$, $n = 7$). Further, in the absence of ANAP, this construct decreased the surface expression of HA-Kir6.2 ($p = 0.009$, $n = 6$) compared to no-SUR1 controls (Fig. S5a), suggesting that channels with SUR truncated at this position may be selectively retained within the cell. Western blots of total protein from cells expressing SUR1-T1397^{amber} in the presence of ANAP and a dominant negative ribosomal release factor[33] confirmed that >95% of SUR1-T1397* was full length (Fig. S5b). The expected distance between T1397

and TNP-nucleotides bound to NBS2 is ~18.3 Å (Fig. 4a), close enough for >99% FRET efficiency (Fig. S2b).

Binding of MgTNP-ADP and MgTNP-ATP to SUR1-T1397*/Kir6.2 (Fig. 4a,b) was qualitatively similar to SUR1-Y1353*/Kir6.2 (Fig. 1, Table 1), although the difference in binding affinity between MgTNP-ADP and MgTNP-ATP was smaller in SUR1-T1397* than SUR1-Y1353*-containing channels. Both TNP-ADP and TNP-ATP bound to SUR1-T1397*/Kir6.2 in the absence of Mg^{2+} (Fig. 4c; Table 1) as we observed for SUR1-Y1353*/Kir6.2.

In excised patches from cells expressing SUR1-T1397*/Kir6.2, we measured robust currents that were inhibited by ATP (Fig. S5c). Interestingly, the apparent affinity for ATP inhibition of for SUR1-T1397*/Kir6.2 was lower than for wild-type K_{ATP} (EC_{50} was 53.9 μM vs. 11.2 μM, respectively; Table 2). More importantly, SUR1-T1397* supported activation of Kir6.2-G334D by both MgADP (Fig. 4d, Table 2) and MgTNP-ADP (Fig. 5, Table 2). The EC_{50} for channel activation by MgTNP-ADP (determined from Hill fits) was 7.3 μM as compared to the EC_{50} of 15.1 μM obtained for MgTNP-ADP binding to NBS2. Although activation (by necessity) was measured with Kir6.2-G334D, and our binding measurements were conducted with wild-type Kir6.2, we do not expect this to have affected our measurements as 1397* is the same distance (~33 Å) as 1353* from the inhibitory binding site on Kir6.2, and expression of SUR1-Y1353* with Kir6.2-G334D did not affect binding measurements (Fig. S3, Table 1).

Discussion

Taken together, our data suggest a modified model for SUR1/Kir6.2 K_{ATP} activation through nucleotide binding to SUR1 (Fig. 6). ADP and ATP bind to NBS2 in the absence of Mg^{2+}. However, without Mg^{2+} as a co-factor, adenine nucleotides cannot dimerize the NBDs and initiate the conformational change in SUR1 required to affect P_{open}. As the NBDs fail to dimerize, nucleotides dissociate rapidly. If both Mg^{2+} and nucleotides are present, the NBDs dimerize, resulting in slower

nucleotide dissociation. NBD dimerization initiates a conformational change in SUR1 that ultimately communicates nucleotide occupancy to the pore, affecting P_{open}. Inhibitory SUs prevent NBD dimerization. Thus, nucleotides dissociate rapidly even in the presence of Mg^{2+} and P_{open} is not affected by nucleotide occupancy at NBS2. KCOs have the opposite effect. They stabilize NBD dimerization, prolonging nucleotide occupancy at NBS2 and channel activation.

Although our data do not offer any direct structural insight into how NBD dimerization propagates to Kir6.2, our ability to measure MgTNP-ADP binding to NBS2 of SUR1 and channel activation under similar conditions furnishes some mechanistic insights into the relationship between nucleotide binding and channel opening. We simultaneously fit the combined data sets for MgTNP-ADP binding to SUR1-T1397*/Kir6.2 and activation of SUR1-T1397*/Kir6.2-G334D currents with several gating models. For each model, equations for binding and P_{open} used common values for K_A (the equilibrium association constant in units of M^{-1}, constrained such that $K_A > 0$), L (the equilibrium constant for the intrinsic opening of unliganded SUR1-T1397*/Kir6.2, fixed to 0.52 based on the measured P_{open} of SUR1/Kir6.2-G334D[26]), and E (the factor by which MgTNP-ADP binding favors activation, constrained to E>1). Goodness of fit was assessed by comparing the residual sum of the squared deviations (RSS) between the data and fit curves. As K_{ATP} channels open in the absence of Mg^{2+} and nucleotides, we excluded any gating models that lacked unliganded opening. None of the available cryo-EM structures[3,4,6,34,35] show any direct interactions between neighboring SUR1 subunits. Therefore, we excluded models in which binding to one SUR1 directly affects binding to the other SUR1 subunits (i.e. with binding cooperativity).

With these assumptions, the best fits to the data were obtained with an extended Monod-Wyman-Changeux model (Fig. 5; $R^2 = 0.97$, RSS = 0.25)[36]. In this model, binding of MgTNP-ADP to each NBS2 of SUR1 is independent and favors pore opening by the same amount. The data in Fig. 5 were fit with the following expressions for binding and activation:

$$\frac{bound}{total} = \frac{LE[ADP]K_A(E[ADP]K_A + 1)^3 + [ADP]K_A([ADP]K_A + 1)^3}{L(E[ADP]K_A + 1)^4 + ([ADP]K_A + 1)^4} \quad (6)$$

$$P_{open,norm} = \frac{\left(\frac{L(E[ADP]K_A+1)^4}{L(E[ADP]K_A+1)^4+([ADP]K_A+1)^4}\right)-\left(\frac{L}{L+1}\right)}{\left(\frac{LE^4}{LE^4+1}-\frac{L}{L+1}\right)} \quad (7).$$

Previous attempts to determine the stoichiometry of Mg-nucleotide activation of K_{ATP}, i.e. how many SUR1 subunits must bind nucleotide in order to activate current, have produced varying results[37-39]. We also fit MgTNP-ADP binding to NBS2 and current activation for SUR1-T1397* with models in which fixed stoichiometries of 1-4 nucleotide-bound SUR1 subunits were necessary to increase P_{open} (Fig. S6). All of these models used the same assumptions as the MWC model in Fig. 5, but none fit the data so well.

Our binding and activation data were determined in separate experiments. Whereas the equations for binding and current activation both have a term (L) representing the intrinsic opening equilibrium, there is no way of knowing the P_{open} of channels in an unroofed membrane. To derive more quantitative values, ideally experiments should be performed using patch-clamp fluorometry in which binding and current are measured simultaneously[40,41]. However, we were unable to obtain inside-out patches from cells expressing SUR1-T1397*/Kir6.2-G334D with sufficient fluorescence intensity to measure reliable spectra. The concentration-response relationship for current activation was normalized to the minimum and maximum current values, as reflected in equation 7. If the true maximum and minimum P_{open} in a given experiment could be accurately determined, then the quantity E could be computed directly from the minimum P_{open} in the absence of ligand, L/(L+1), and the maximum P_{open} at saturating nucleotide concentrations, $E^4L/(E^4L+1)$. This would be of particular use as the error in our estimate of E is quite high. In practice, however, these values are difficult to measure for K_{ATP} in the presence of Mg^{2+} as channel rundown from loss of PIP_2 results in an intrinsic P_{open} (L) that is constantly changing[42]. Nevertheless, our analysis provides useful qualitative information regarding the mechanism by which nucleotide binding to NBS2 of SUR1 activates Kir6.2.

The affinities we measured for (Mg)TNP-ADP and (Mg)TNP-ATP binding are higher than those previously estimated for (Mg)ATP and (Mg)ADP from photoaffinity labeling studies on SUR1 in the

absence of Kir6.2[43] or from ATPase assays preformed on isolated NBD2 fusion proteins[44]. This may reflect a higher affinity of TNP nucleotides for NBS2 of SUR1 compared to ATP and ADP, as observed for other ABC transporters[23] or the absence of Kir6.2. Nevertheless, the EC_{50} values obtained from MgTNP-ATP and MgTNP-ADP binding to SUR1-Y1353*/Kir6.2 were in reasonably good agreement with those measured for MgATP and MgADP activation of SUR1/Kir6.2-G334D currents[26]. It is unlikely that the introduction of ANAP modified the binding affinity of NBS2 as the apparent affinity for TNP-nucleotides in the absence of Mg^{2+} was unaffected by the site at which ANAP was inserted (Table 1). The difference in apparent affinities between SUR1-Y1353* and SUR1-T1397* in the presence of Mg^{2+} may indicate a difference in the ability of bound nucleotides to promote NBD dimerization.

Our ability to separate effects on nucleotide binding from channel activation will be of considerable value for future investigations. They will allow us to address the role of nucleotide binding at NBS1 and Kir6.2, and explore the mechanistic ramifications of disease-associated K_{ATP} mutations. Furthermore, simultaneous binding and current measurements will yield precise information regarding the coupling of stimulatory and inhibitory nucleotide binding to the channel pore. This coupling of ligand binding to an effector domain (the channel pore) that lies tens of Å away provides an excellent model for studying long-range communication within protein complexes. It has also not escaped our notice that our method is readily adaptable to the study of other ABC proteins, ATP-gated channels like P2X receptors, and any protein for which there is a suitable fluorescent ligand.

Materials and Methods

Molecular Biology. Human SUR1 and human Kir6.2 were subcloned into pcDNA4/TO (Invitrogen; Carlsbad, CA) for expression in HEK-293T cells. To obtain GFP-labeled channels, SUR1 was cloned into pCGFP_EU[45]. Mutagenesis, including insertion of amber (TAG) stop codons, was performed using the QuikChange kit (Agilent; Santa Clara, CA) or by subcloning synthetic oligonucleotides (Sigma; St. Louis, MO) between convenient restriction sites. All clones were verified by sequencing (DNA Sequencing and Services; Dundee, Scotland). pCDNA4/TP and pANAP were obtained from Addgene.

pERF1-E55D and pCGFP_EU were kind gifts from the Chin Laboratory (MRC Laboratory of Molecular Biology, Cambridge UK) and Gouaux Laboratory (Vollum Institute, Portland OR USA), respectively.

Cell Culture and Expression of Fluorescently Tagged Protein. HEK-293T cells (ATTC; Manassas, VA) were grown in 6-well plates (STARLAB; Milton Keynes, UK) or 30 mm culture dishes (STARLAB) on untreated 30 mm borosilicate coverslips (Thickness # 1, VWR International; Radnor, PA) or on poly-D-lysine coated FluoroDishes (FD35-PDL-100, World Precision Instruments; Hitchin, UK) in Dulbecco's Modified Eagle Medium (Sigma) supplemented with 10% fetal bovine serum, 100 U/mL penicillin, and 100 µg/mL streptomycin (Thermo Fisher Scientific; Waltham, MA) at 37ºC, 5%/95% CO_2/air.

SUR1 constructs were site-specifically tagged with the fluorescent amino acid ANAP using amber codon suppression as described by Chatterjee *et al.*[17]. 30 mm dishes of HEK 293T cells were co-transfected with pANAP (0.5-1 µg), Kir6.2 (0.5 µg), and SUR1 (1-1.5 µg) constructs containing an amber stop codon (TAG) at amino acid position 1353 or 1397 (1353^{amber} or 1397^{amber}) using TransIT transfection reagent (Mirus Bio LLC; Madison, WI) in a ratio of 3 µL of TransIT per µg of total DNA. Following transfection the media was supplemented with 20 µM ANAP (free acid or methyl ester). pANAP encodes a tRNA/tRNA synthetase pair specific for ANAP. In the presence of ANAP, cells transfected with pANAP generate tRNAs charged with ANAP that recognize the amber stop codon. Thus, full-length ANAP-tagged SUR can be produced. Proper co-assembly of Kir6.2 subunits with SUR1 subunits is ensured by the fact that the two subunits rely on one another for proper exit from the ER and trafficking to the plasma membrane[32]. An exception to this may be SUR1_GFP, which has been shown to traffic independently of Kir6.2[46]. After transfection, cells were cultured at 33º C, 5%/95% CO_2/air to slow growth and increase the per-cell protein yield[47]. To enhance expression of full-length, ANAP-labeled proteins, 1-2 µg of a plasmid containing a dominant negative eukaryotic release factor 1 (pERF1-E55D) was included in the transfection mix as indicated[33]. Experiments were typically performed 2-5 days post transfection.

Preparation of unroofed membrane fragments for imaging. Unroofed membranes were prepared using a modification of a protocol from the Heuser laboratory[19-21]. Briefly, a coverslip containing adherent cells was removed from the cell culture media and a small piece (0.5-1 cm) was broken off using jewelers forceps (#5) and washed in phosphate buffered saline (PBS, Thermo Fisher Scientific) diluted 1:3 in deionized water. Cells were exposed 3x10 s to a solution of 0.01% poly-L-lysine (Sigma) with intervening washes in diluted PBS to adhere them more firmly to the coverslips. The coverslip fragment was then placed in a 30 mm culture dish filled with 2-3 mL of 1/3X PBS and sonicated very briefly (~100 ms) using a probe sonicator (Vibra-cell), leaving behind adherent plasma membrane and sometimes additional cellular material. The unroofed fragments in our experiments were sometimes visible under bright-field illumination, a potential result of our modified "unroofing" procedure. Morphologically, such cell fragments resemble the "partially unroofed" cells identified by Usukura *et al.*[20]. Cells cultured on poly-D-lysine coated FluoroDishes were unroofed in diluted PBS with no additional poly-L-lysine treatment. This procedure yielded a higher percentage of completely unroofed plasma membranes (i.e. nearly invisible with brightfield illumination).

Microscopy/spectroscopy Unroofed membrane fragments were imaged directly on FluoroDishes (FD35-PDL-100, World Precision Instruments) or on broken coverslips placed in a FluoroDish (FD3510, World Precision instruments) using a Nikon TE2000-U microscope equipped with a 40x (S Fluor, 1.3 NA, Nikon) or 100x (Apo TIRF, 1.49 NA, Nikon; Kingston Upon Thames, UK) oil-immersion objective and low-fluorescence immersion oil (MOIL-30, Olympus; Southend-on-Sea, UK) or a 60x water immersion objective (Plan Apo VC, 1.20 NA, Nikon). ANAP was excited using a ThorLabs LED source (LED4D067) at 385 nm connected to the microscope using a liquid light guide with a 390/18 nm band-pass filter (MF390-18, ThorLabs; Newton, NJ) and MD416 dichroic (ThorLabs). For imaging, emitted light was filtered through a 479/40 nm band-pass filter (MF479-40, ThorLabs). GFP was imaged using a similar setup with excitation at 490 nm, a 480/40 band-pass excitation filter (Chroma; Bellows Falls, VT), a DM505 dichroic mirror (Chroma), and 510 nm long-pass emission filter. For spectroscopy, ANAP was

excited as above, but emitted light was passed through a 400 nm long-pass filter (FEL0400, ThorLabs) and directed through the slit of an Isoplane 160 spectrometer (300 g/mm grating; Princeton Instruments; Trenton, NJ). Spectral images (spatial information on the *y*-axis and wavelength on the *x*-axis) were acquired using a PIXIS 400B CCD camera (Princeton Instruments) attached to the spectrograph (Fig. S1c). Exposure times were typically 100 ms for brightfield images, 1-10 s for steady-state spectra and 1-5 s for time-course experiments. The emission spectrum of ANAP-labeled SUR1 showed a peak around 470 nm, which was used to differentiate labeled channels from autofluorescence (which typically had a broad emission spectrum), from cytoplasmic ANAP (or potentially ANAP-conjugated to tRNA), which peaks ~480 nm or from bright, fluorescent debris on the coverslip which was morphologically distinct from unroofed membranes and had spectra peaking at either ~450 nm or 480-485 nm.

To verify that the fluorescence signal we observed in unroofed membrane fragments derived from SUR1-Y1353*, we co-transfected cells with Kir6.2 and GFP-tagged SUR1 with or without an amber stop codon at position Y1353. After unroofing, membranes from transfected cells could be identified by the green fluorescence of SUR1_GFP/Kir6.2. Fig. S1b shows that membranes expressing SUR1_GFP-Y1353*/Kir6.2 were brightly fluorescent for both GFP and ANAP, whereas those from SUR1_GFP expressing cells had only GFP fluorescence. We also acquired emission spectra from membranes expressing SUR1_GFP-Y1353*/Kir6.2 (Fig. S1c). The intensity of the ANAP peak in our fluorescence was linearly proportional to the peak GFP fluorescence, and the intensity of the ANAP peak at zero GFP (i.e. no expression of SUR1_GFP-Y1353*) was zero. Taken together, these data suggest that non-specific ANAP background was very low. We also performed Western blotting on FLAG-tagged SUR1-$Y1353^{amber}$ constructs to verify that we produced full-length, ANAP-labeled SUR1, and that cells were unable to read through the amber stop codon to produce full-length protein in the absence of ANAP (Fig. S1d).

To prevent accumulation of fluorescent nucleotides in the bath, FluoroDishes were perfused with either (in mM) 140 KCl, 20 NaCl, 10 $MgCl_2$, 10 HEPES pH 7.2 w/NaOH or 140 KCl, 20 NaCl, 1 EDTA,

10 HEPES pH 7.2 w/NaOH using a peristaltic pump (Ismatec). Unroofed membranes were directly perfused with nucleotides using an 8-channel µFlow perfusion system (ALA Scientific Instruments; Farmingdale, NY). Solution change with the µFlow was rapid (τ = 0.73 s ±0.02 s) as measured from single exponential fits to wash-out of 50 µM tetramethylrhodamine-5-maleimide (TMRM) after switching to a solution with 0 TMRM. TMRM was excited with a 565 nm LED with a D540/25X band-pass filter (Chroma) and DM565 dichroic mirror (Chroma). Emitted light was collected through a D605/55M band-pass filter (Chroma).

Images and spectra were acquired using LightField (Princeton Instruments). The solution changer, camera, and light source were all controlled using pClamp 10.5 (Molecular Devices; San Jose, CA) and a DigiData 1440 A/D converter. All data were acquired at room temperature (18º-22º C).

Analysis of images and spectra. Images were adjusted and displayed using Fiji[48]. Spectra were analyzed using custom code written in Matlab (Mathworks; Natick, MA). Regions of interest corresponding to fluorescent membrane fragments were manually selected from the spectral images and averaged for each wavelength. A background region of similar size was selected and the average was subtracted from the spectrum of the region of interest. The peak fluorescence (~470 nm) was automatically selected by determining the maximum of a boxcar average of 31 points (corresponding to ~10 nm) of the data in the absence of nucleotides. Data were corrected for photobleaching by fitting an exponential decay to the normalized peak of 5-6 images acquired prior to washing on TNP-nucleotides and dividing the raw spectra by the resulting fit at each cumulative exposure time. Corrected data were normalized by the peak ANAP fluorescence at 0 [TNP-nucleotide] (F/F_{max}) and displayed as $1-F/F_{max}$. On occasion data were normalized instead to the fluorescence at 50 nM nucleotide, as we consistently saw no effect at this concentration. TNP-nucleotide concentration-response relationships were fit with the Hill equation

$$\mathbf{1} - \frac{\boldsymbol{F}}{\boldsymbol{F_{max}}} = \boldsymbol{E_{max}} * \frac{[\boldsymbol{TNP}]^{\boldsymbol{h}}}{\boldsymbol{EC_{50}}^{\boldsymbol{h}} + [\boldsymbol{TNP}]^{\boldsymbol{h}}} \quad (\mathbf{1})$$

where E_{max} is the FRET efficiency at saturating concentrations, [*TNP*] is the concentration of TNP-nucleotide, EC_{50} is the half-maximal concentration and *h* is the Hill slope.

To generate the plot of GFP fluorescence vs. ANAP fluorescence in Fig. S1c, spectra of ANAP and GFP tagged SUR1 subunits expressed in unroofed membrane fragments were acquired as above. We were able to resolve a GFP peak at 510 nm with 385 nm excitation, even though this wavelength is far from the λ_{max} for GFP. It is possible that GFP emission was enhanced via FRET between ANAP and GFP. The ANAP peak fluorescence at 470 nm did not overlap with the GFP emission peak. However, the peak GFP at 510 nm was contaminated by the shoulder of the ANAP peak. Therefore, the GFP fluorescence was corrected by subtracting the averaged (from 16 membranes) fluorescence of ANAP incorporated into SUR1, scaled to match the 470 nm peak in the ANAP-GFP spectrum.

To measure the time course of nucleotide unbinding, the fluorescence at the TNP-nucleotide peak (usually around 560 nm) was plotted as a function of time after exchanging to a zero-nucleotide solution, as following the time course of the rise in ANAP fluorescence was complicated by photobleaching. After complete wash out of nucleotides, the fluorescence at 560 nm was non zero, as the shoulder of the ANAP emission spectrum extends into the range of wavelengths at which TNP-nucleotides emit. Therefore, the time course data were corrected by subtracting a linear fit to the data following complete washout. This corrected for the shoulder of the ANAP spectrum as well as the continued photobleaching of ANAP. Data were normalized to the maximum fluorescence at t = 0 and fit with single-exponential decays

$$\frac{F}{F_{max}} = e^{-t/\tau} \quad (2)$$

or double-exponential decays

$$\frac{F}{F_{max}} = A_1 e^{-t/\tau_1} + A_2 e^{-t/\tau_2} \quad (3).$$

Wash-out time courses following exchange to [TNP-nucleotide] = 0 should be independent of the nucleotide concentration before wash. The majority of our time-course experiments were conducted at the conclusion of our concentration-response experiments, and therefore reflect wash after applying a concentration of 1 mM. For experiments in diazoxide and tolbutamide, the nucleotide concentration prior to wash was 50 μM.

In some experiments, there was evidence of cross-contamination of our wash solution or low-nucleotide solutions via back-flow of solutions with higher concentrations of nucleotide (as evident by accumulation of yellow TNP-nucleotides). We excluded data from such experiments and maintained/replaced valves on the μFlow as needed.

Electrophysiology. Currents were recorded from inside-out membrane patches excised from transfected HEK-293T cells. Pipettes were pulled to a resistance of 1-5 MΩ and filled with an extracellular solution containing (in mM) 140 KCl, 1.2 $MgCl_2$, 2.6 $CaCl_2$, and 10 HEPES, pH 7.4 or 140 KCl, 1 EGTA, 10 HEPES, pH 7.3. The intracellular (bath) solutions contained either (in mM) 107 KCl, 2 $MgCl_2$, 1 $CaCl_2$, 10 EGTA, and 10 HEPES, pH 7.2 or 140 KCl, 1 EDTA, 1 EGTA, 10 HEPES pH 7.3. Nucleotides were added as indicated. Patches were perfused with an 8-channel μFlow perfusion system. Data were acquired at a holding potential of -60 mV using an Axopatch 200B amplifier and Digidata 1322A digitizer with pClamp 9.0 software (Molecular Devices). Currents were digitized at 10 kHz and low-pass filtered at 1 kHz. K_{ATP} channels rundown in excised patches (reviewed by Proks *et al.*[42]). For inhibitory concentration-response relationships, rundown was corrected by alternating test nucleotide solutions with nucleotide-free (control) solutions and expressing the test currents as a fraction of the average of the control currents before and after the test solution and fit to the following expression:

$$\frac{I}{I_{max}} = 1 - \frac{[TNP]^h}{EC_{50}{}^h + [TNP]^h} \quad (4).$$

For activation concentration-responses, the same protocol was used, but test concentrations were alternated with a saturating concentration (1 mM) of MgADP[26]. Data were displayed at the current magnitude in the test concentration minus the current in zero nucleotide ($I-I_{min}$) divided by the current in saturating nucleotide (1 mM MgADP) minus the current in zero nucleotide ($I_{max} - I_{min}$) and fit to the following expression:

$$\frac{I - I_{min}}{I_{max} - I_{min}} = \frac{[TNP]^h}{{EC_{50}}^h + [TNP]^h} \quad (5)$$

Currents were leak corrected by subtracting the remaining current after complete rundown.

Western Blotting. In order to detect SUR1 via Western blot, a 3xFLAG (MDYKDHDGDYKDHDIDYKDDDDK) tagged construct (tag in an extracellular loop between amino acid positions T1042 and L1043) was used (SUR1-3xFLAG) with or without amber stop codons at amino acid positions 1353 or 1397. HEK-293T cells were transfected in 6-well plates using the conditions described above, but with 1 µg of SUR1 DNA. After 48 h, cells were washed and harvested with gentle pipetting in 1 mL of PBS (Sigma). Cells were pelleted (4 min at 0.2 x *g* yielding 20-50 mg pellets) and solubilized in 50-100 µL of 0.5% Triton X-100 in 110 mM potassium acetate, buffered at pH 7.4. 125 U of benzonase (Sigma) was added to each sample and samples were incubated at room temperature for 20 min. 7.5 µL of each sample was mixed with 2.5 µL of NuPAGE LDS sample buffer and 1 µL NuPAGE sample reducing agent (Invitrogen) and run on a NuPAGE 4-12% Bis-Tris gel (Invitrogen) at 200 V for 40 min in 1X MOPS-SDS buffer (Invitrogen). Protein was transferred overnight at 10 V to an Immobilon-P membrane (Merck Millipore; Burlington, MA) in 25 mM Tris, 192 mM glycine, and 20% methanol + 0.1% SDS. Following transfer, the membrane was rinsed in TBS-Tw (150 mM NaCl, 25 mM Tris, pH 7.2, and 0.05% Tween 20) and incubated (with shaking) for 30 min in 5% milk in TBS-Tw. The membrane was rinsed three times in TBS-Tw and incubated for 30 min with primary antibody (M2 anti-FLAG from Sigma, diluted 1:500 in TBS-Tw). The membrane was rinsed three more times in TBS-Tw

and incubated for 30 min with secondary antibody (HRP-conjugated sheep anti-mouse IgG, GE Healthcare Life Sciences; Freiburg, Germany) diluted 1:20,000 in TBS-Tw + 1% milk. Finally, the membrane was rinsed 3x10 min in TBS-Tw and developed using SuperSignal West Femto Max Sensitivity Substrate (Thermo Fisher Scientific). Images were collected using a C-DiGit scanner (Licor Biosciences; Lincoln NE) and band intensities were quantified using custom code written in MATLAB.

Western blotting was performed (Fig. S1d) on the total protein from HEK-293T cells transfected with Kir6.2 and 3xFLAG-tagged SUR1-Y1353^{amber} DNA under various conditions. As the 3xFLAG tag was N-terminal to SUR1, we used it to probe for both full-length and truncated SUR1. As a positive control, we transfected 3x-FLAG-tagged SUR1 with no stop codon, which was only expected to produce full-length protein (lane 1). This protein ran above our 140 kDa marker as expected (predicted MW is ~180 kDa). In the absence of ANAP or in cells transfected without the pANAP plasmid, only truncated 3xFLAG-SUR1 protein was evident (lanes 4 and 5), confirming that there was no full-length protein produced by accidental read-through of the amber (TAG) codon. In the presence of both pANAP and ANAP, we obtained a mixture of full-length (66%) and truncated (34%) SUR1. The majority of our experiments in unroofed membrane fragments were performed under such conditions as the signals we measured (fluorescence) were derived solely from full-length (i.e. ANAP-labeled) channels. Finally, we were able to increase expression of full-length SUR1 as needed by transfecting an additional plasmid, pERF1-E55D, which encodes a dominant negative ribosomal release factor[33]. With the additional expression of ERF1-E55D, we obtained 92% full-length protein (Fig. S1d).

In parallel experiments, we expressed SUR1_GFP-Y1353^{amber} in the absence of ANAP. Under such conditions, we observed a few cells with diffuse GFP fluorescence throughout the cytoplasm. We believe that the signal from such cells was derived from soluble GFP generated from an internal methionine after position 1353 and not read-through of the amber stop codon, as the distribution of this protein differed from that of SUR1_GFP (which was confined to the plasma membrane and presumably ER/Golgi). We never observed GFP fluorescence in unroofed membranes of such cells.

Surface Expression Assay. Surface expression of SUR1 constructs was assayed by their ability to chaperone HA-tagged Kir6.2 subunits to the plasma membrane using an adaptation of the method of Zerangue *et al.*[32]. The HA tag plus linker (YAYMEKGITDLAYPYDVPDY) was inserted in the extracellular region following helix M1 of Kir6.2 between amino acids L100 and A101. HEK-293T cells were cultured in 12-well plates (STARLAB) on 19 mm cover slips treated with poly-L-lysine. Transfections were performed as described above, but DNA amounts were adjusted for the smaller scale (0.08 µg HA-tagged Kir6.2, 0.14 µg SUR1 constructs, 0.14 µg pANAP, 0.14 µg pERF1-E55D). Cells were incubated in DMEM (+10% FBS, 100 U/mL penicillin, and 100 µg/mL streptomycin) at 33ºC in a 95% air/5% CO_2 atmosphere for 48 hours in the presence or absence (as indicated) of 20 µM ANAP. Following incubation, cells were rinsed on ice with PBS and fixed for 30 min in PBS + 10% neutral buffered formalin. Cells were subsequently washed twice in PBS and blocked with 1% bovine serum albumin (BSA) in PBS for 30 min at 4º C. Cells were then incubated for 1 h at 4º C in PBS + 1% BSA with a 1:1000 dilution of rat anti-HA monoclonal antibody (Roche; Basel, Switzerland) and washed 5x10 min on ice with PBS + 1% BSA. HRP-conjugated goat anti-rat polyclonal antibody (diluted 1:2000, Jackson ImmunoResearch; Ely, UK) was applied in PBS + 1% BSA and cells were incubated an additional 30 min at 4º C. Finally, cells were washed 4x10 min in PBS + 1% BSA and 5x10 min in PBS on ice. After the wash, coverslips were removed from PBS and placed in clean, untreated 35 mm culture dishes. 300 µL of SuperSignal ELISA Femto Maximum Sensitivity Substrate (Thermo Fisher Scientific) were added and the luminescence was measured using a Glomax 20/20 Luminometer (Promega; Madison, WI) after a 10 s incubation. For display purposes, data were normalized to the mean of the luminescence with wild-type SUR1. Background was assessed with cells that were transfected with HA-tagged Kir6.2, but no SUR1.

Chemicals. ANAP trifluoroacetate salt and methyl ester were obtained from Asis Chemicals (Waltham, MA). A 1 mM stock of the salt was prepared in 30 mM NaOH and stored at -80º C. The methyl ester was dissolved at 5 mM in DMSO and stored at -20º C. The two forms were used interchangeably, as the final

product (when ANAP is incorporated into a protein) is identical and in our experience both free acid and methyl ester were membrane permeant. Trinitrophenyl (TNP) nucleotide analogues were purchased from Jena Bioscience (Jena, Germany). 1 mM stocks were prepared in buffer and stored at -20º C. Stocks were verified using UV-Vis spectroscopy (Beckman Coulter DU800 spectrophotometer; Pasadena, CA) as needed. Paper chromatography (mobile phase 40:10:25 *n*-butanol, glacial acetic acid: H_2O) was used to verify that older TNP-ATP stocks had not undergone hydrolysis. All other chemicals were from Sigma. Diazoxide was prepared in a 34 mM stock in 100 mM KOH and stored at -20º C before use. Tolbutamide was dissolved at 100 mM in DMSO and stored at -20º C.

Data presentation and statistics. All data were plotted as mean ±SEM, with the exception of the box plots in Fig. 2e and Fig. S5a, the boxes of which represented ±SD. The number of experiments (n) represents the number of patches or membranes used in a given experiment. For surface expression assays, n represents the number of transfected coverslips. Plots and curve fitting were generated using Origin 9.1 (OriginLab Corporation; Northampton, MA). Curves in the figures (and parameters reported in the figure legends) represent fits to the combined data sets, with errors representing the standard error of the fits. Shaded regions indicate 95% confidence intervals. Fit parameters reported in Tables are the mean ±SEM (Tables 1 and 2) or ±SD (Table 3) of the fits to individual experiments. Pairwise comparisons were performed using two-tailed Student's *t*-tests with the Welch correction (not assuming equal variance) and the Bonferroni correction for multiple comparisons, as needed. Comparisons of EC_{50} values were performed on log-transformed data as the untransformed EC_{50} is not normally distributed.

Acknowledgments

We wish to thank Idoia Portillo and Raul Terron Exposito for excellent technical assistance and Gregor Sachse, Chris Miller, and David Gadsby for helpful discussions. James Cantley provided access to the Western blot scanner. This work was supported by the European Research Council (grant 332620),

the Biotechnology and Biological Sciences Research Council (BB/R002517/1), the John Fell Fund, and the Wellcome Trust Oxion graduate program.

Competing Interests

We declare no competing interests.

Figure Legends

Figure 1. Measuring binding to NBS2 of SUR1. **(a)** Cartoon illustrating the topology of the K_{ATP} channel complex. Two (of four) Kir6.2 subunits and one (of four) SUR1 subunits are shown for clarity. The locations of the inhibitory (red, on Kir6.2) and stimulatory (green, on SUR1) NBSs are indicated. **(b)** Chemical structures of TNP-ATP and ANAP. The fluorescent moiety is colored in each. **(c)** Structure of the ligand-bound NBDs of SUR1 (from PDB accession # 6C3O)[3]. TNP-ATP (from PDB accession # 3AR7)[49] was positioned in both NBSs of SUR1 by alignment with MgATP (at NBS1) and MgADP (at NBS2), which were present in the original structure. Y1353 from the A-loop of NBS2 is highlighted in yellow to mark the location of ANAP in our experiments. Alignment of TNP-ATP with nucleotides bound to NBS1 and NBS2 in the cryo-EM structure of SUR1 does not predict any structural clashes. **(d)** Representative spectral images acquired from an unroofed membrane fragment expressing SUR1-Y1353*/Kir6.2 channels in the absence or presence of increasing concentrations of TNP-ADP. **(e)** Averaged spectra from (d). **(f)** Concentration-response relationships for binding of MgTNP-ATP (magenta) and MgTNP-ADP (cyan) to SUR1-Y1353*/Kir6.2. Data were fit to equation 1. MgTNP-ATP: E_{max} = 1.00 ±0.05, EC_{50} = 29.3 μM ±6.5 μM, h = 0.8 ±0.1. MgTNP-ADP: E_{max} = 0.99 ±0.02, EC_{50} = 4.8 μM ±0.5 μM, h = 0.8 ±0.1. **(g)** Concentration-response relationships for binding of TNP-ATP and TNP-ADP to SUR1-Y1353*/Kir6.2 channels in the absence of Mg^{2+}. TNP-ATP: E_{max} = 0.84 ±0.04, EC_{50} = 8.5 μM ±2.4 μM, h = 0.8 ±0.1. TNP-ADP: E_{max} = 0.95 ±0.02, EC_{50} = 6.1 μM ±0.7 μM, h = 0.8 ±0.1. Increasing the concentration of TNP-ADP to 10 mM did not significantly change the amount of quenching (n = 3, data not shown).

Figure 2. Conditions that favor channel opening slow nucleotide dissociation from NBS2. **(a)** Average dissociation time course of TNP-ADP from SUR1-Y1353*/Kir6.2 K_{ATP} channels in the presence (orange) and absence (gray) of Mg^{2+}. Combined data from multiple experiments were fit to single exponential decays (equation 2). TNP-ADP: τ = 4.2 s ±0.2 s; MgTNP-ADP: τ = 21.3 s ±0.8 s. **(b)** Dissociation time course of TNP-ATP from SUR1-Y1353*/Kir6.2 channels in the presence and absence of Mg^{2+}.

Dissociation of TNP-ATP in the absence of Mg^{2+} was better fit with a bi-exponential decay (equation 3). TNP-ATP: τ_1 = 4.5 s ±0.9 s, A_1 = 0.65 ±0.06, τ_2 = 28.2 s ±3.7 s, A_2 = 0.35 ±0.06, n = 7; MgTNP-ATP: τ = 15.0 s ±0.5 s. **(c,d)** Dissociation time course of MgTNP-ADP (c) or MgTNP-ATP (d) from SUR1-Y1353*/Kir6.2 in the presence of 500 µM tolbutamide (pink) or 340 µM diazoxide (teal). (c) The orange curve is the fit to the MgTNP-ADP data from (a). Tolbutamide: τ = 6.4 s ±0.2 s; diazoxide: τ = 52.6 s ±1.4 s. (d) The orange curve is the fit to MgTNP-ATP data from (b). Tolbutamide: τ = 6.3 s ±0.1 s; diazoxide: τ = 60.5 s ±1.4 s. **(e)** Time to 50% dissociation ($t_{0.5}$) for the individual fits to the data shown in (a)-(d) for better comparison between single-exponential and more complex time courses. Boxes represent mean ±SD. Individual data points are shown to the right of the boxes.

Figure 3. Mutation of the Walker$_A$ motif of NBS1 affects apparent the affinity for MgTNP-ADP. **(a)** Interaction of the Walker$_A$ lysine (K1384) with MgADP bound to NBS2 of SUR1 (from PDB accession # 6C3O)[3]. The K1384A (K2A) mutation (modeled *below*) disrupts this interaction. **(b)** Binding of TNP-ATP to SUR1-Y1353*,K2A/Kir6.2 K_{ATP} channels in the absence of Mg^{2+}. Data were fit to equation 1. E_{max} = 0.87 ±0.03, EC_{50} = 4.3 µM ±0.1 µM, h = 0.9 ±0.2. Gray curves are fits to SUR1-Y1353*/Kir6.2 channels from Fig. 1. **(c)** Binding of TNP-ADP to SUR1-Y1353*,K2A/Kir6.2 in the absence of Mg^{2+}. E_{max} = 0.91 ±0.02, EC_{50} = 4.4 µM ±0.1 µM, h = 0.9 ±0.1. **(d)** Binding of MgTNP-ATP to SUR1-Y1353*,K2A/Kir6.2. E_{max} = 0.97 ±0.06, EC_{50} = 21.5 µM ±6.7 µM, h = 0.8 ±0.1. **(e)** Binding of MgTNP-ADP to SUR1-Y1353*,K2A/Kir6.2. E_{max} = 0.96 ±0.04, EC_{50} = 16.5 µM ±4.2 µM, h = 1.1 ±0.2. **(f)** Dissociation time course of MgTNP-ADP from SUR1-Y1353*,K2A/Kir6.2 (green). Data were fit to a single exponential; τ = 13.5 s ±0.3 s. Fits to the dissociation of TNP-ADP from SUR1-Y1353*/Kir6.2 in the presence (orange) and absence (gray) of Mg^{2+} from Fig. 2 are shown for comparison.

Figure 4. Binding of TNP-nucleotides to SUR1-T1397*/Kir6.2 K_{ATP} channels. (a) Structure of the ligand-bound NBDs of SUR1 (from PDB accession # 6C3O)[3] with TNP-ATP aligned as in Fig. 1c. T1397 in NBD2 is highlighted in yellow to mark the placement of ANAP in our experiments. **(b)** Concentration-response relationships for binding of MgTNP-ATP (magenta) and MgTNP-ADP (cyan) to SUR1-

T1397*/Kir6.2 channels. Data were fit to equation 1. MgTNP-ATP: E_{max} = 1.00 ±0.02, EC_{50} = 14.7 μM ±1.8 μM, h = 1.0 ±0.1. MgTNP-ADP: E_{max} = 1.0 ±0.02, EC_{50} = 11.4 μM ±1.4 μM, h = 0.9 ±0.1. **(c)** Concentration-response relationships for binding of TNP-ATP and TNP-ADP to SUR1-Y1397*/Kir6.2 channels in the absence of Mg^2. TNP-ATP: E_{max} = 0.94 ±0.02, EC_{50} = 4.8 μM ±0.7 μM, h = 0.8 ±0.1. TNP-ADP: E_{max} = 0.98 ±0.05, EC_{50} = 5.6 μM ±1.7 μM, h = 0.7 ±0.1. **(d)** Activation of SUR1-T1397*/Kir6.2-G334D channels by MgADP in inside-out patches. Data were fit with equation 5. EC_{50} = 386 μM ±5.8 μM, h = 1.2 ±0.2.

Figure 5. Activation of K_{ATP} by Mg-nucleotide binding at SUR1 proceeds via an MWC-type reaction. Combined data for MgTNP-ADP binding (cyan from Fig. 4b; SUR1-T1397*/Kir6.2) and current activation (gray from SUR1-T1397*/Kir6.2-G334D in separate experiments, n = 6) were fit simultaneously with MWC expressions for binding (equation 6) and activation (equation 7) with shared parameters for the two expressions. Note the overlapping gray and cyan curves from the fits. The schematic on the right describes the MWC model. Closed K_{ATP} channels are drawn as squares and open channels as circles. Filled symbols represent subunits bound to MgTNP-ADP (abbreviated as MgADP). Channels open by a concerted flip of all four subunits. L = 0.52, E = 1.2 ±1.3, and K_A = 1.1x10^5 M^{-1} ±6.2x10^4 M^{-1}. Each MgTNP-ADP binding event is independent and each MgTNP-ADP-bound NBS2 contributes equally to increase P_{open}.

Figure 6. Schematic for activation of K_{ATP} by nucleotide binding to SUR1. **(*top, left*)** In the absence of Mg^{2+} nucleotides bind and rapidly dissociate from the NBSs of SUR1, without affecting its conformation. Nucleotide occupancy of SUR1 is not communicated to Kir6.2. **(*top, right*)** In the presence of both Mg^{2+} and nucleotide, the NBD dimer interface is stabilized. This interface must open in order for nucleotides to leave, so nucleotide dissociation is greatly slowed. NBD dimerization requires a conformational change in the transmembrane domain of SUR1. This conformational change is communicated to Kir6.2 to increase the favorability of channel opening. **(*bottom, left*)** Sulfonylureas prevent the conformational change in the transmembrane domain of SUR1 and preclude NBD dimerization. Therefore, nucleotide dissociation is

rapid, even in the presence of Mg^{2+} and no increase in open probability results from Mg-nucleotide binding to SUR1. **(*bottom, right*)** Potassium channel openers stabilize the closed-dimer conformation of the NBDs. As a result, nucleotide dissociation is very slow and channel activation is enhanced.

Supplementary Figure S1. ANAP fluorescence is specific to SUR-Y1353* in unroofed membrane fragments. **(a)** *above*. Brightfield (BF) and fluorescence images of an unroofed membrane fragment from an HEK-293T cell expressing SUR1-Y1353*/Kir6.2. The dashed line indicates the position of the spectrograph slit. *below*. Image of the fluorescence from the same membrane after the light was diffracted by the gratings of the spectrograph. Spatial information in the *y* dimension is preserved. Spatial information in the *x* dimension is replaced by wavelength. **(b)** Brightfield (BF) and fluorescence images of unroofed membrane fragments from HEK-293T cells expressing SUR1_GFP-Y1353*/Kir6.2 (*above*) and SUR1_GFP/Kir6.2 (*below*). Fluorescence images were acquired and scaled identically for each fluorophore. **(c)** Intensity of ANAP fluorescence as a function of GFP fluorescence (n = 34). Data were fit with a straight line with the intercept fixed to 0 and a slope of 0.96 ±0.02 (R = 0.99). **(d)** Western blot for 3xFLAG-tagged SUR1 subunits expressed in HEK-293T cells. All cells were co-transfected with Kir6.2. Unless otherwise indicated, all cells were cultured in 20 μM ANAP. The first lane (positive control) was 3xFLAG_SUR1 with no amber stop codon at position 1353, which shows only full-length protein. The next two lanes show 3xFLAG_SUR1-Y1353^{amber} co-transfected with pANAP and pERF1-E55D (92% full-length SUR1), or with pANAP alone (66% full-length SUR1). Omission of pANAP (lane 3) or ANAP (lane 4) resulted in only truncated protein. Background signal is shown in the last two lanes in which either no SUR1 was transfected or untagged SUR1 was used. The positions of the full-length and truncated protein (at amino acid 1352) are marked. Upper bands (~260 kDa and higher) are from aggregated SUR1 protein.

Supplementary Figure S2. TNP-nucleotides are suitable for measuring nucleotide binding to K_{ATP}. **(a)** Overlap between the absorbance spectrum of TNP-ADP (green) and the emission spectrum of ANAP (cyan) when incorporated into SUR1 (SUR1-Y1353*/Kir6.2) and measured in unroofed membrane

fragments. **(b)** Theoretical FRET efficiency as a function of distance calculated from the spectral overlap shown in (a). Half maximal FRET efficiency (R_0) occurs at 43 Å. κ^2 was assumed to be 0.67 (i.e. random orientation between the donor and acceptor was assumed). **(c)** Representative trace showing activation of SUR1/Kir6.2-G334D K_{ATP} channels in an excised patch by MgADP and MgTNP-ADP. **(d)** Activation of SUR1/Kir6.2-G334D currents by MgTNP-ADP. Data were fit to equation 5. EC_{50} = 22.1 µM ±3.0 µM, h = 0.9 ±0.1, n = 7. **(e)** MgTNP-ATP "binding" to an unroofed membrane fragment from an HEK-293 cell transfected with pANAP (but no Kir6.2 or SUR1) and incubated in media with 20 µM ANAP. No ANAP fluorescence was observed, but non-specific MgTNP-ATP fluorescence was observed at nucleotide concentrations of 500 µM and higher. **(f)** Spectra of SUR1-Y1353*/Kir6.2 channels in an unroofed membrane fragment in the absence or presence of 10 mM MgATP. The intensity in 10 mM MgATP was 98% ±2% of the original peak (n = 7) and 101% ±2% in 10 mM MgADP (n = 8).

Supplementary Figure S3. Mutation of the inhibitory nucleotide site in Kir6.2 does not affect binding measured at NBS2 of SUR1. **(a)** Proximity of the inhibitory NBS of Kir6.2 to NBS2 of SUR1 in the Mg-nucleotide-bound structure of K_{ATP} (PDB accession # 6C3O)[3]. TNP-ATP (from PDB accession # 3AR7)[49] was aligned with ATP in the original structure. The dashed line represents a distance of 33 Å. **(b)** Concentration-response relationship for binding of MgTNP-ADP to SUR1-Y1353*/Kir6.2-G334D channels in the presence of Mg^{2+}. Data were fit with equation 1: E_{max} = 0.99 ±0.04, EC_{50} = 8.6 µM ±1.7 µM, h = 1.0 ±0.2. The concentration-response relationship for MgTNP-ADP binding to SUR1-Y1353*/Kir6.2 channels from Fig. 1f is shown in gray.

Supplementary Figure S4. Mg^{2+} effects on steady-state nucleotide binding. **(a)** Concentration-response relationships for TNP-ADP binding to SUR1-Y1353*/Kir6.2 in the presence and absence of Mg^{2+}. **(b)** Concentration-response relationships for TNP-ATP binding to SUR1-Y1353*/Kir6.2 in the presence and absence of Mg^{2+}. Data and fits are repeated from Fig. 1.

Supplementary Figure S5. SUR1-T1397*/Kir6.2 K_{ATP} channels traffic to the plasma membrane and form functional channels. **(a)** Chemiluminescence assay for surface expression of HA-tagged Kir6.2 in

the presence and absence of SUR1, in SUR1-Y1353^{amber}-transfected HEK-293T cells cultured in the presence or absence of 20 μM ANAP, and in SUR1-T1397^{amber} transfected HEK-293T cells cultured in the presence or absence of 20 μM ANAP. **(b)** Western blot for 3xFLAG-tagged SUR1 subunits expressed in HEK-293T cells. All cells were co-transfected with Kir6.2 and cultured in the presence of 20 μM ANAP. Two separate experiments are shown. In each, the positive control was 3xFLAG_SUR1 with no amber stop codon. The negative control was SUR1 with no FLAG tag. The next two lanes show 3xFLAG_SUR1-T1397^{tag} co-transfected with pANAP and pERF1-E55D, or with pERF1-E55D and no pANAP. The positions of the full-length and truncated (at amino acid 1396) proteins are marked. **(c)** Inhibition of SUR1-T1397*/Kir6.2 (gray) and SUR1/Kir6.2 (brown) channels by ATP in the absence of Mg^{2+} measured in inside-out patches. Data were fit to equation 4. SUR1-T1397*: EC_{50} = 49.2 μM ±4.7 μM, h = -1.1 ±0.1. SUR1: EC_{50} = 11.1 μM ±6.5 μM, h = -1.3 ±0.1.

Supplementary Figure S6. Fits to alternate gating models. Binding and gating data from Fig. 5 fit to alternative models. Fit parameters are shown as insets. Goodness of fit was assessed as the residual sum of squares (RSS). **(a)** MWC model as in Fig. 5. **(b)** Model in which binding of MgADP to a single SUR1 is sufficient to increase channel activity.

$$\frac{bound}{total} = \frac{LE[ADP]K_A(1 + 3[ADP]K_A + 3[ADP]^2K_A^2 + [ADP]^3K_A^3) + [ADP]K_A([ADP]K_A + 1)^3}{L(1 + 4E[ADP]K_A + 6E[ADP]^2K_A^2 + 4E[ADP]^3K_A^3 + E[ADP]^4K_A^4) + ([ADP]K_A + 1)^4}$$

$$P_{open,norm} = \frac{\left(\frac{L(1 + 4E[ADP]K_A + 6E[ADP]^2K_A^2 + 4E[ADP]^3K_A^3 + E[ADP]^4K_A^4)}{L(1 + 4E[ADP]K_A + 6E[ADP]^2K_A^2 + 4E[ADP]^3K_A^3 + E[ADP]^4K_A^4) + ([ADP]K_A + 1)^4}\right) - \left(\frac{L}{L+1}\right)}{\left(\frac{LE}{LE+1} - \frac{L}{L+1}\right)}$$

(c) Model in which binding of MgADP to two SUR1 subunits is required to increase channel activity.

$$\frac{bound}{total} = \frac{L[ADP]K_A(1 + 3E[ADP]K_A + 3E[ADP]^2K_A^2 + E[ADP]^3K_A^3) + [ADP]K_A([ADP]K_A + 1)^3}{L(1 + 4[ADP]K_A + 6E[ADP]^2K_A^2 + 4E[ADP]^3K_A^3 + E[ADP]^4K_A^4) + ([ADP]K_A + 1)^4}$$

$$P_{open,norm} = \frac{\left(\frac{L(1 + 4[ADP]K_A + 6E[ADP]^2K_A^2 + 4E[ADP]^3K_A^3 + E[ADP]^4K_A^4)}{L(1 + 4[ADP]K_A + 6E[ADP]^2K_A^2 + 4E[ADP]^3K_A^3 + E[ADP]^4K_A^4) + ([ADP]K_A + 1)^4}\right) - \left(\frac{L}{L+1}\right)}{\left(\frac{LE}{LE+1} - \frac{L}{L+1}\right)}$$

(d) Model in which binding of MgADP to three SUR1 subunits is required to increase channel activity.

$$\frac{bound}{total} = \frac{L[ADP]K_A(1 + 3[ADP]K_A + 3E[ADP]^2K_A^2 + E[ADP]^3K_A^3) + [ADP]K_A([ADP]K_A + 1)^3}{L(1 + 4[ADP]K_A + 6[ADP]^2K_A^2 + 4E[ADP]^3K_A^3 + E[ADP]^4K_A^4) + ([ADP]K_A + 1)^4}$$

$$P_{open,norm} = \frac{\left(\frac{L(1 + 4[ADP]K_A + 6[ADP]^2K_A^2 + 4E[ADP]^3K_A^3 + E[ADP]^4K_A^4)}{L(1 + 4[ADP]K_A + 6[ADP]^2K_A^2 + 4E[ADP]^3K_A^3 + E[ADP]^4K_A^4) + ([ADP]K_A + 1)^4}\right) - \left(\frac{L}{L+1}\right)}{\left(\frac{LE}{LE+1} - \frac{L}{L+1}\right)}$$

(e) Model in which all four SUR1 subunits must be occupied by MgADP in order to increase channel open probability.

$$\frac{bound}{total} = \frac{L[ADP]K_A(1 + 3[ADP]K_A + 3[ADP]^2K_A^2 + E[ADP]^3K_A^3) + [ADP]K_A([ADP]K_A + 1)^3}{L(1 + 4[ADP]K_A + 6[ADP]^2K_A^2 + 4[ADP]^3K_A^3 + E[ADP]^4K_A^4) + ([ADP]K_A + 1)^4}$$

$$P_{open,norm} = \frac{\left(\frac{L(1 + 4[ADP]K_A + 6[ADP]^2K_A^2 + 4[ADP]^3K_A^3 + E[ADP]^4K_A^4)}{L(1 + 4[ADP]K_A + 6[ADP]^2K_A^2 + 4[ADP]^3K_A^3 + E[ADP]^4K_A^4) + ([ADP]K_A + 1)^4}\right) - \left(\frac{L}{L+1}\right)}{\left(\frac{LE}{LE+1} - \frac{L}{L+1}\right)}$$

References

1. Ashcroft, F.M. & Rorsman, P. K(ATP) channels and islet hormone secretion: new insights and controversies. *Nat Rev Endocrinol* **9**, 660-9 (2013).

2. Quan, Y., Barszczyk, A., Feng, Z.P. & Sun, H.S. Current understanding of K ATP channels in neonatal diseases: focus on insulin secretion disorders. *Acta Pharmacol Sin* **32**, 765-80 (2011).

3. Lee, K.P.K., Chen, J. & MacKinnon, R. Molecular structure of human KATP in complex with ATP and ADP. *Elife* **6**(2017).

4. Martin, G.M., Kandasamy, B., DiMaio, F., Yoshioka, C. & Shyng, S.L. Anti-diabetic drug binding site in a mammalian KATP channel revealed by Cryo-EM. *Elife* **6**(2017).

5. Puljung, M.C. Cryo-electron microscopy structures and progress toward a dynamic understanding of KATP channels. *J Gen Physiol* **150**, 653-669 (2018).

6. Wu, J.X., Ding, D., Wang, M., Kang, Y., Zeng, X. & Chen, L. Ligand binding and conformational changes of SUR1 subunit in pancreatic ATP-sensitive potassium channels. *Protein Cell* **9**, 553-567 (2018).

7. Inagaki, N., Gonoi, T., Clement, J.P.t., Namba, N., Inazawa, J., Gonzalez, G., Aguilar-Bryan, L., Seino, S. & Bryan, J. Reconstitution of IKATP: an inward rectifier subunit plus the sulfonylurea receptor. *Science* **270**, 1166-70 (1995).

8. Sakura, H., Ammala, C., Smith, P.A., Gribble, F.M. & Ashcroft, F.M. Cloning and functional expression of the cDNA encoding a novel ATP-sensitive potassium channel subunit expressed in pancreatic beta-cells, brain, heart and skeletal muscle. *FEBS Lett* **377**, 338-44 (1995).

9. Aguilar-Bryan, L., Nichols, C.G., Wechsler, S.W., Clement, J.P.t., Boyd, A.E., 3rd, Gonzalez, G., Herrera-Sosa, H., Nguy, K., Bryan, J. & Nelson, D.A. Cloning of the beta cell high-affinity sulfonylurea receptor: a regulator of insulin secretion. *Science* **268**, 423-6 (1995).

10. Inagaki, N., Gonoi, T. & Seino, S. Subunit stoichiometry of the pancreatic beta-cell ATP-sensitive K+ channel. *FEBS Lett* **409**, 232-6 (1997).

11. Tucker, S.J., Gribble, F.M., Zhao, C., Trapp, S. & Ashcroft, F.M. Truncation of Kir6.2 produces ATP-sensitive K+ channels in the absence of the sulphonylurea receptor. *Nature* **387**, 179-83 (1997).

12. Nichols, C.G., Shyng, S.L., Nestorowicz, A., Glaser, B., Clement, J.P.t., Gonzalez, G., Aguilar-Bryan, L., Permutt, M.A. & Bryan, J. Adenosine diphosphate as an intracellular regulator of insulin secretion. *Science* **272**, 1785-7 (1996).

13. Gribble, F.M., Tucker, S.J. & Ashcroft, F.M. The interaction of nucleotides with the tolbutamide block of cloned ATP-sensitive K+ channel currents expressed in Xenopus oocytes: a reinterpretation. *J Physiol* **504 (Pt 1)**, 35-45 (1997).

14. Gribble, F.M., Tucker, S.J. & Ashcroft, F.M. The essential role of the Walker A motifs of SUR1 in K-ATP channel activation by Mg-ADP and diazoxide. *EMBO J* **16**, 1145-52 (1997).

15. Ashcroft, F.M., Puljung, M.C. & Vedovato, N. Neonatal Diabetes and the KATP Channel: From Mutation to Therapy. *Trends Endocrinol Metab* **28**, 377-387 (2017).

16. Matsuo, M., Kioka, N., Amachi, T. & Ueda, K. ATP binding properties of the nucleotide-binding folds of SUR1. *J Biol Chem* **274**, 37479-82 (1999).

17. Chatterjee, A., Guo, J., Lee, H.S. & Schultz, P.G. A genetically encoded fluorescent probe in mammalian cells. *J Am Chem Soc* **135**, 12540-3 (2013).

18. Ueda, K., Komine, J., Matsuo, M., Seino, S. & Amachi, T. Cooperative binding of ATP and MgADP in the sulfonylurea receptor is modulated by glibenclamide. *Proc Natl Acad Sci U S A* **96**, 1268-72 (1999).

19. Heuser, J. The production of 'cell cortices' for light and electron microscopy. *Traffic* **1**, 545-52 (2000).

20. Usukura, J., Yoshimura, A., Minakata, S., Youn, D., Ahn, J. & Cho, S.J. Use of the unroofing technique for atomic force microscopic imaging of the intra-cellular cytoskeleton under aqueous conditions. *J Electron Microsc (Tokyo)* **61**, 321-6 (2012).

21. Zagotta, W.N., Gordon, M.T., Senning, E.N., Munari, M.A. & Gordon, S.E. Measuring distances between TRPV1 and the plasma membrane using a noncanonical amino acid and transition metal ion FRET. *J Gen Physiol* **147**, 201-16 (2016).

22. Lopez-Alonso, J.P., de Araujo, E.D. & Kanelis, V. NMR and fluorescence studies of drug binding to the first nucleotide binding domain of SUR2A. *Biochemistry* **51**, 9211-22 (2012).

23. Oswald, C., Jenewein, S., Smits, S.H., Holland, I.B. & Schmitt, L. Water-mediated protein-fluorophore interactions modulate the affinity of an ABC-ATPase/TNP-ADP complex. *J Struct Biol* **162**, 85-93 (2008).

24. Vanoye, C.G., MacGregor, G.G., Dong, K., Tang, L., Buschmann, A.S., Hall, A.E., Lu, M., Giebisch, G. & Hebert, S.C. The carboxyl termini of K(ATP) channels bind nucleotides. *J Biol Chem* **277**, 23260-70 (2002).

25. Drain, P., Li, L. & Wang, J. KATP channel inhibition by ATP requires distinct functional domains of the cytoplasmic C terminus of the pore-forming subunit. *Proc Natl Acad Sci U S A* **95**, 13953-8 (1998).

26. Proks, P., de Wet, H. & Ashcroft, F.M. Activation of the K(ATP) channel by Mg-nucleotide interaction with SUR1. *J Gen Physiol* **136**, 389-405 (2010).

27. Corry, B., Jayatilaka, D. & Rigby, P. A flexible approach to the calculation of resonance energy transfer efficiency between multiple donors and acceptors in complex geometries. *Biophys J* **89**, 3822-36 (2005).

28. Proks, P., de Wet, H. & Ashcroft, F.M. Sulfonylureas suppress the stimulatory action of Mg-nucleotides on Kir6.2/SUR1 but not Kir6.2/SUR2A KATP channels: a mechanistic study. *J Gen Physiol* **144**, 469-86 (2014).

29. Gribble, F.M., Reimann, F., Ashfield, R. & Ashcroft, F.M. Nucleotide modulation of pinacidil stimulation of the cloned K(ATP) channel Kir6.2/SUR2A. *Mol Pharmacol* **57**, 1256-61 (2000).

30. de Wet, H., Shimomura, K., Aittoniemi, J., Ahmad, N., Lafond, M., Sansom, M.S. & Ashcroft, F.M. A universally conserved residue in the SUR1 subunit of the KATP channel is essential for translating nucleotide binding at SUR1 into channel opening. *J Physiol* **590**, 5025-36 (2012).

31. Magge, S.N., Shyng, S.L., MacMullen, C., Steinkrauss, L., Ganguly, A., Katz, L.E. & Stanley, C.A. Familial leucine-sensitive hypoglycemia of infancy due to a dominant mutation of the beta-cell sulfonylurea receptor. *J Clin Endocrinol Metab* **89**, 4450-6 (2004).

32. Zerangue, N., Schwappach, B., Jan, Y.N. & Jan, L.Y. A new ER trafficking signal regulates the subunit stoichiometry of plasma membrane K(ATP) channels. *Neuron* **22**, 537-48 (1999).

33. Schmied, W.H., Elsasser, S.J., Uttamapinant, C. & Chin, J.W. Efficient multisite unnatural amino acid incorporation in mammalian cells via optimized pyrrolysyl tRNA synthetase/tRNA expression and engineered eRF1. *J Am Chem Soc* **136**, 15577-83 (2014).

34. Li, N., Wu, J.X., Ding, D., Cheng, J., Gao, N. & Chen, L. Structure of a Pancreatic ATP-Sensitive Potassium Channel. *Cell* **168**, 101-110 e10 (2017).

35. Martin, G.M., Yoshioka, C., Rex, E.A., Fay, J.F., Xie, Q., Whorton, M.R., Chen, J.Z. & Shyng, S.L. Cryo-EM structure of the ATP-sensitive potassium channel illuminates mechanisms of assembly and gating. *Elife* **6**(2017).

36. Monod, J., Wyman, J. & Changeux, J.P. On the Nature of Allosteric Transitions: A Plausible Model. *J Mol Biol* **12**, 88-118 (1965).

37. Babenko, A.P. A novel ABCC8 (SUR1)-dependent mechanism of metabolism-excitation uncoupling. *J Biol Chem* **283**, 8778-82 (2008).

38. Hosy, E. & Vivaudou, M. The unusual stoichiometry of ADP activation of the KATP channel. *Front Physiol* **5**, 11 (2014).

39. Tammaro, P., Girard, C., Molnes, J., Njolstad, P.R. & Ashcroft, F.M. Kir6.2 mutations causing neonatal diabetes provide new insights into Kir6.2-SUR1 interactions. *EMBO J* **24**, 2318-30 (2005).

40. Biskup, C., Kusch, J., Schulz, E., Nache, V., Schwede, F., Lehmann, F., Hagen, V. & Benndorf, K. Relating ligand binding to activation gating in CNGA2 channels. *Nature* **446**, 440-3 (2007).

41. Zheng, J. & Zagotta, W.N. Gating rearrangements in cyclic nucleotide-gated channels revealed by patch-clamp fluorometry. *Neuron* **28**, 369-74 (2000).

42. Proks, P., Puljung, M.C., Vedovato, N., Sachse, G., Mulvaney, R. & Ashcroft, F.M. Running out of time: the decline of channel activity and nucleotide activation in adenosine triphosphate-sensitive K-channels. *Philos Trans R Soc Lond B Biol Sci* **371**(2016).

43. Matsuo, M., Tanabe, K., Kioka, N., Amachi, T. & Ueda, K. Different binding properties and affinities for ATP and ADP among sulfonylurea receptor subtypes, SUR1, SUR2A, and SUR2B. *J Biol Chem* **275**, 28757-63 (2000).

44. de Wet, H., Mikhailov, M.V., Fotinou, C., Dreger, M., Craig, T.J., Venien-Bryan, C. & Ashcroft, F.M. Studies of the ATPase activity of the ABC protein SUR1. *FEBS J* **274**, 3532-44 (2007).

45. Kawate, T. & Gouaux, E. Fluorescence-detection size-exclusion chromatography for precrystallization screening of integral membrane proteins. *Structure* **14**, 673-81 (2006).

46. Makhina, E.N. & Nichols, C.G. Independent trafficking of KATP channel subunits to the plasma membrane. *J Biol Chem* **273**, 3369-74 (1998).

47. Lin, C.Y., Huang, Z., Wen, W., Wu, A., Wang, C. & Niu, L. Enhancing Protein Expression in HEK-293 Cells by Lowering Culture Temperature. *PLoS One* **10**, e0123562 (2015).

48. Schindelin, J., Arganda-Carreras, I., Frise, E., Kaynig, V., Longair, M., Pietzsch, T., Preibisch, S., Rueden, C., Saalfeld, S., Schmid, B., Tinevez, J.Y., White, D.J., Hartenstein, V., Eliceiri, K., Tomancak, P. & Cardona, A. Fiji: an open-source platform for biological-image analysis. *Nat Methods* **9**, 676-82 (2012).

49. Toyoshima, C., Yonekura, S., Tsueda, J. & Iwasawa, S. Trinitrophenyl derivatives bind differently from parent adenine nucleotides to Ca2+-ATPase in the absence of Ca2+. *Proc Natl Acad Sci U S A* **108**, 1833-8 (2011).

construct	nucleotide	E_{max}	EC_{50} (μM)	h	n
SUR1-Y1353*/Kir6.2	MgTNP-ADP	0.99 ± 0.01	5.5 ± 0.9	0.77 ± 0.03	8
	MgTNP-ATP	0.99 ± 0.02	37.5 ± 11.9	0.86 ± 0.07	7
	ADP	0.95 ± 0.01	6.8 ± 1.3	0.79 ± 0.04	7
	ATP	0.83 ± 0.03	12.8 ± 5.6	0.88 ± 0.06	7
SUR1-Y1353*,K2A/Kir6.2	MgTNP-ADP	0.98 ± 0.03	19.6 ± 10.5	0.91 ± 0.04	5
	MgTNP-ATP	0.99 ± 0.02	31.4 ± 9.1	1.1 ± 0.3	6
	ADP	0.92 ± 0.02	5.0 ± 1.0	0.88 ± 0.05	6
	ATP	0.90 ± 0.03	8.1 ± 3.8	0.98 ± 0.13	6
SUR1-T1397*/Kir6.2	MgTNP-ADP	1.03 ± 0.03	15.1 ± 4.6	0.93 ± 0.09	6
	MgTNP-ATP	1.00 ± 0.01	17.1 ± 3.9	1.0 ± 0.1	10
	ADP	0.98 ± 0.02	6.3 ± 2.3	0.84 ± 0.13	9
	ATP	0.94 ± 0.01	4.7 ± 0.8	0.83 ± 0.09	8
SUR1-Y1353*/Kir6.2-G334D	MgTNP-ADP	1.01 ± 0.03	8.2 ± 1.9	0.90 ± 0.16	5

Table 1. Mean ± SEM from individual fits of equation 1 to nucleotide binding data.

construct	nucleotide	EC50 (μM)	h	n
SUR1/Kir6.2	ATP	11.2 ± 0.1	-1.3 ± 0.1	6
SUR1-T1397*/Kir6.2	ATP	53.9 ± 9.4	-1.2 ± 0.1	6
SUR1/Kir6.2-G334D	MgTNP-ADP	20.6 ± 0.4	1.1 ± 0.2	12
SUR1-T1397*/Kir6.2-G334D	MgTNP-ADP	7.3 ± 1.2	1.0 ± 0.1	5
	MgADP	44.4 ± 14.5	1.5 ± 0.3	5

Table 2. Mean ± SEM from individual fits of equations 4 and 5 to electrophysiological data.

SUR1 construct	nucleotide	drug	$T_{0.5}$ (s)	n
Y1353*	TNP-ADP		2.9 ± 0.5	7
	MgTNP-ADP		14.7 ± 4.2	7
	MgTNP-ADP	tolbutamide	4.5 ± 1.5	7
	MgTNP-ADP	diazoxide	36.9 ± 9.4	7
	TNP-ATP		4.8 ± 1.5	7
	MgTNP-ATP		10.5 ± 1.9	7
	MgTNP-ATP	tolbutamide	4.4 ± 1.6	7
	MgTNP-ATP	diazoxide	42.0 ± 9.7	6
Y1353*,K2A	MgTNP-ADP		9.3 ± 2.1	4

Table 3. Mean ± SD from exponential fits to nucleotide wash-out time courses.

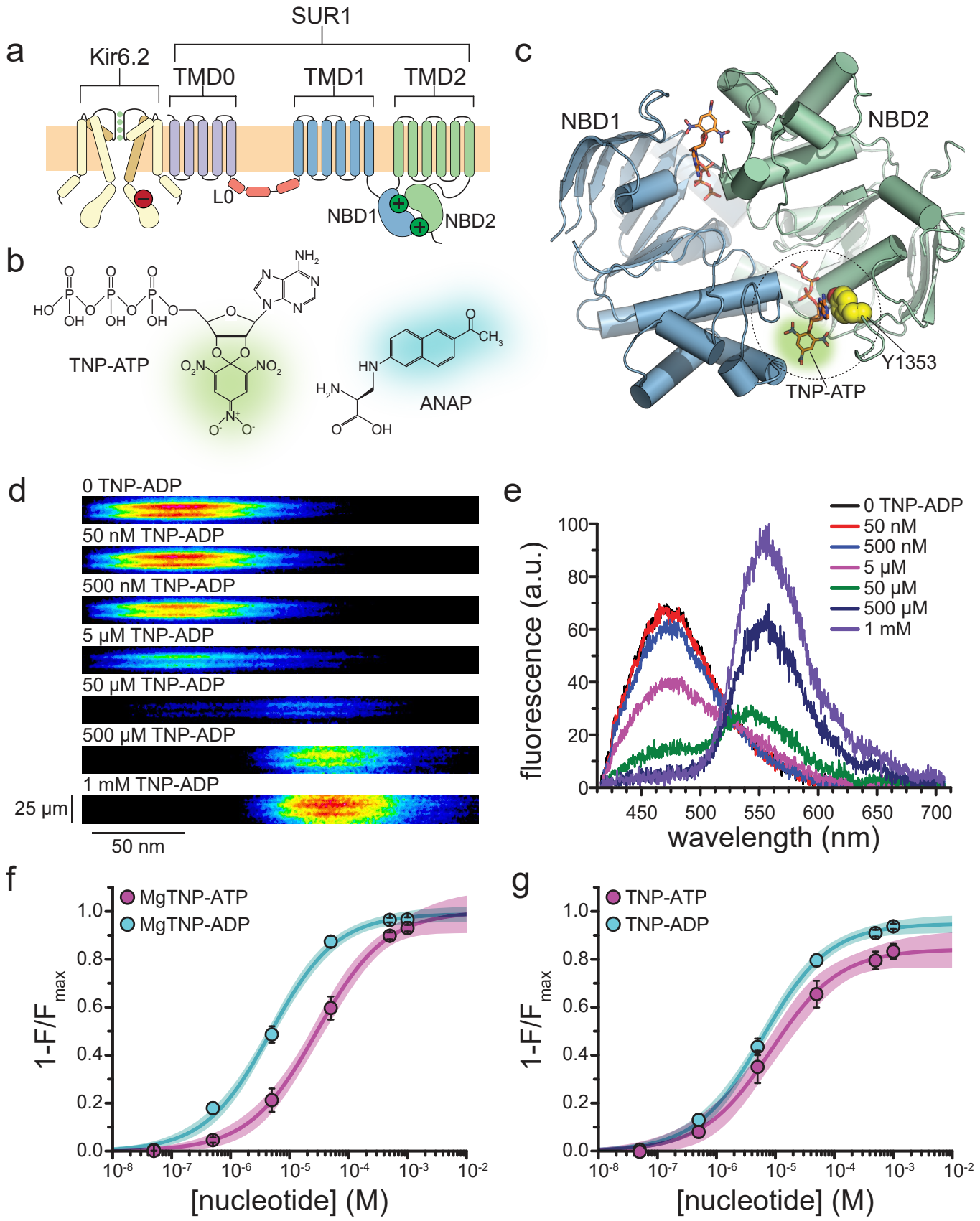
a
SUR1
Kir6.2
TMD0
TMD1
TMD2
L0
NBD1
NBD2
b
TNP-ATP
ANAP
c
NBD1
NBD2
Y1353
TNP-ATP
d
0 TNP-ADP
50 nM TNP-ADP
500 nM TNP-ADP
5 μM TNP-ADP
50 μM TNP-ADP
500 μM TNP-ADP
1 mM TNP-ADP
25 μm
50 nm
e
0 TNP-ADP
50 nM
500 nM
5 μM
50 μM
500 μM
1 mM
fluorescence (a.u.)
wavelength (nm)
f
MgTNP-ATP
MgTNP-ADP
1-F/F max
[nucleotide] (M)
g
TNP-ATP
TNP-ADP
1-F/F max
[nucleotide] (M)

Figure 1

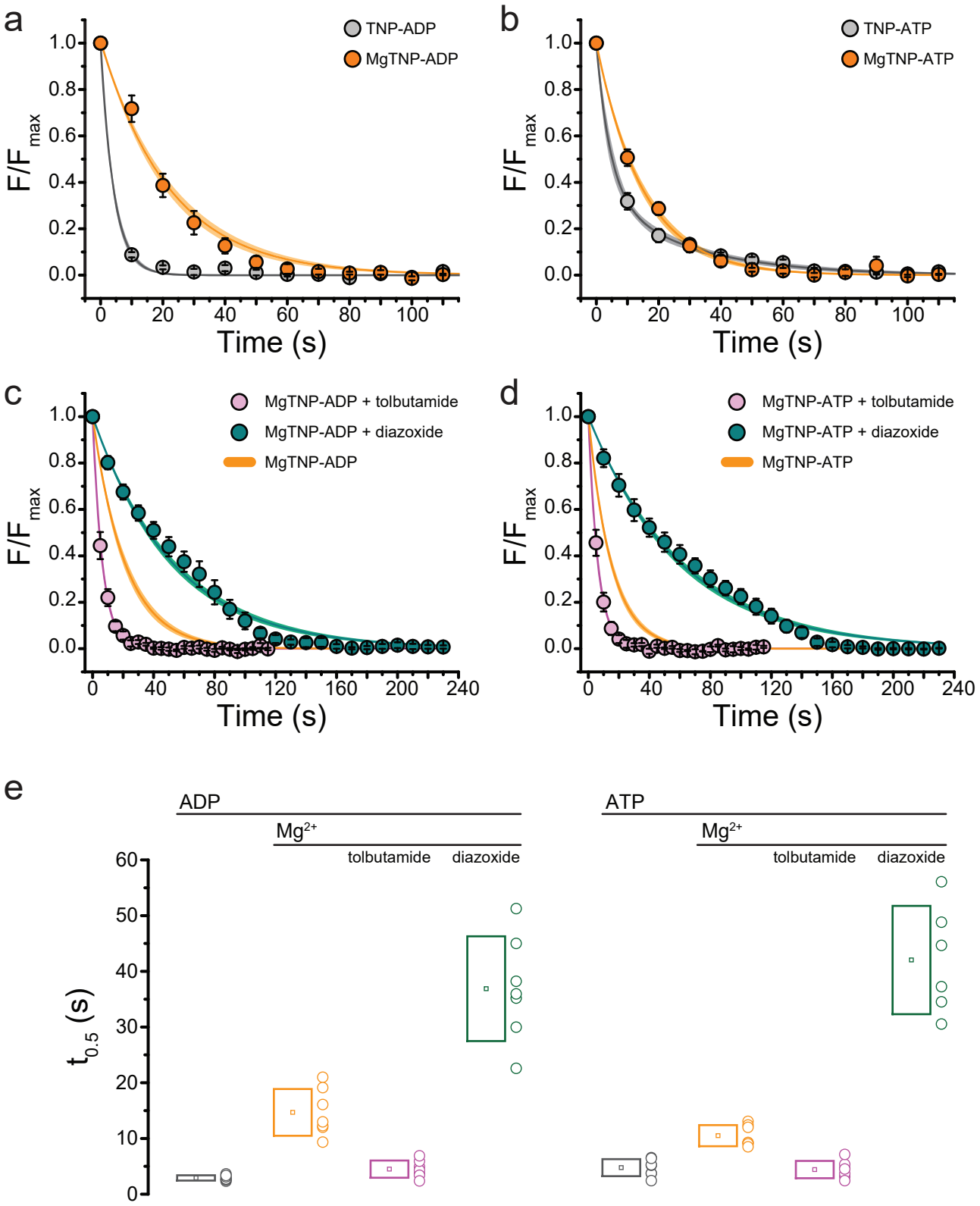
a
TNP-ADP
MgTNP-ADP
F/F max
Time (s)
b
TNP-ATP
MgTNP-ATP
F/F max
Time (s)
c
MgTNP-ADP + tolbutamide
MgTNP-ADP + diazoxide
MgTNP-ADP
F/F max
Time (s)
d
MgTNP-ATP + tolbutamide
MgTNP-ATP + diazoxide
MgTNP-ATP
F/F max
Time (s)
e
ADP
Mg2+
tolbutamide
diazoxide
ATP
Mg2+
tolbutamide
diazoxide
t0.5 (s)

Figure 2

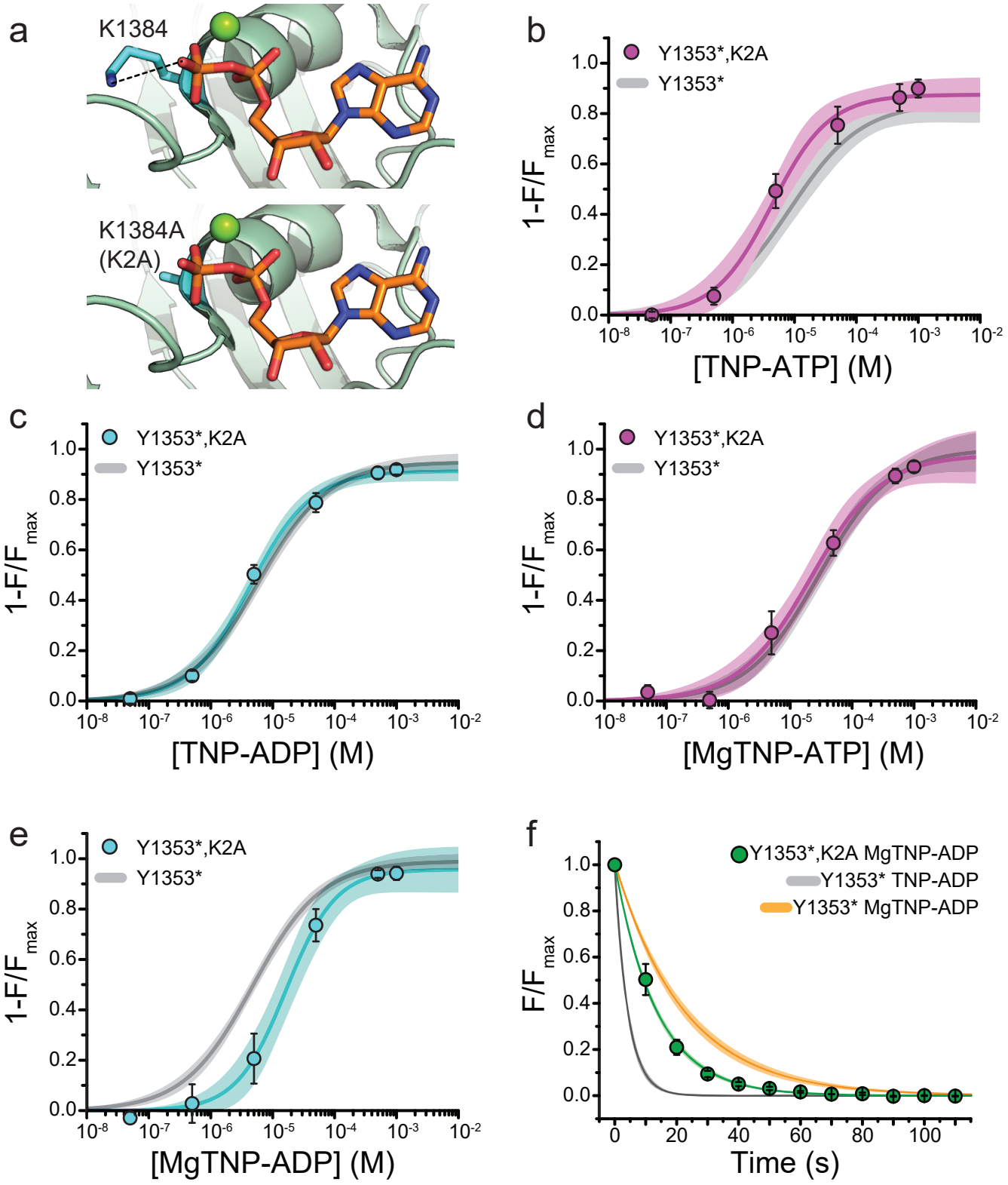
a
K1384
K1384A
(K2A)
b
Y1353*,K2A
Y1353*
1-F/F max
[TNP-ATP] (M)
c
Y1353*,K2A
Y1353*
1-F/F max
[TNP-ADP] (M)
d
Y1353*,K2A
Y1353*
1-F/F max
[MgTNP-ATP] (M)
e
Y1353*,K2A
Y1353*
1-F/F max
[MgTNP-ADP] (M)
f
Y1353*,K2A MgTNP-ADP
Y1353* TNP-ADP
Y1353* MgTNP-ADP
F/F max
Time (s)

Figure 3

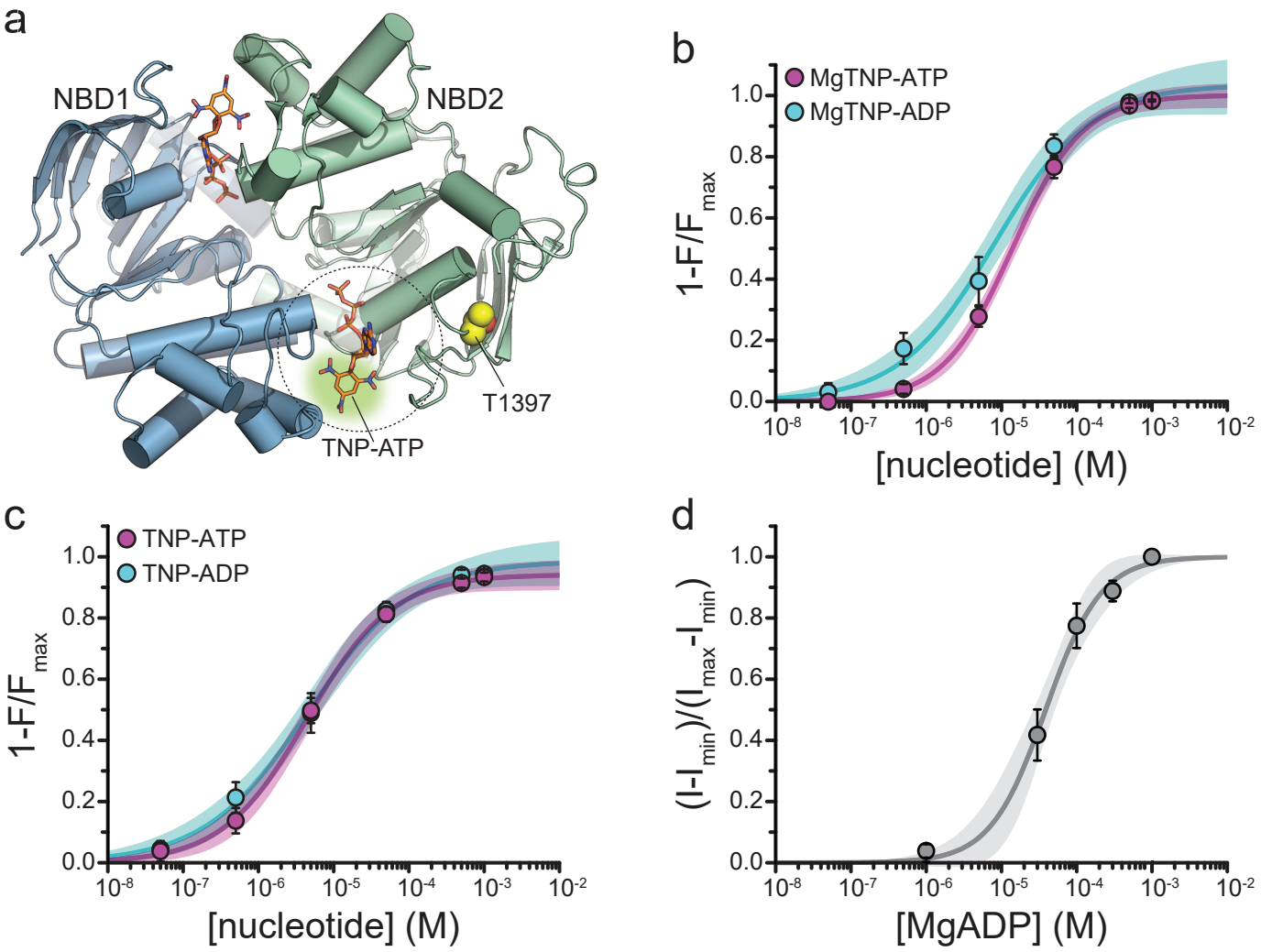
a
NBD1
NBD2
T1397
TNP-ATP
b
MgTNP-ATP
MgTNP-ADP
1-F/F$_{max}$
[nucleotide] (M)
c
TNP-ATP
TNP-ADP
1-F/F$_{max}$
[nucleotide] (M)
d
(I-I$_{min}$)/(I$_{max}$-I$_{min}$)
[MgADP] (M)

Figure 4

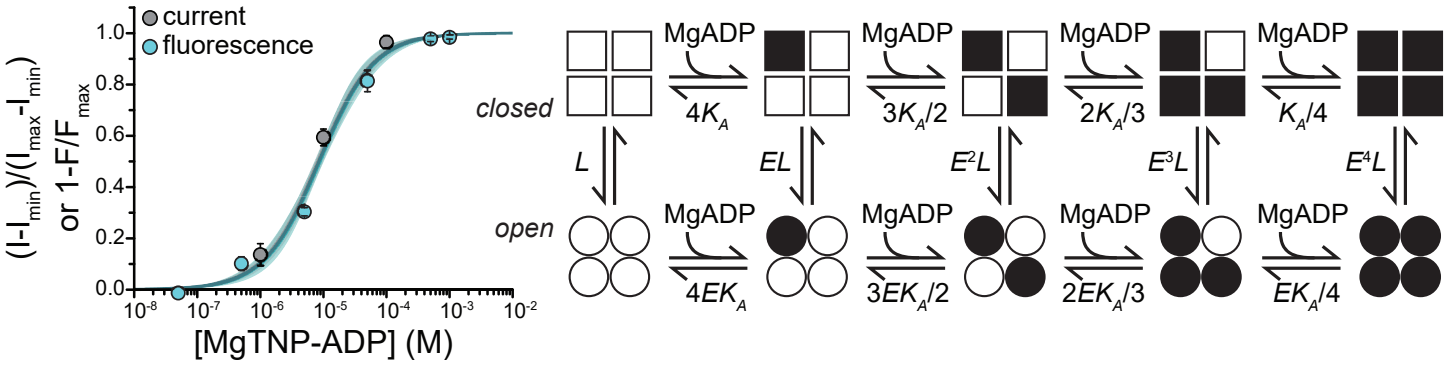
current
fluorescence
(I-I_min)/(I_max-I_min)
or 1-F/F_max
1.0
0.8
0.6
0.4
0.2
0.0
10^-8
10^-7
10^-6
10^-5
10^-4
10^-3
10^-2
[MgTNP-ADP] (M)
closed
open
MgADP
4K_A
3K_A/2
2K_A/3
K_A/4
L
EL
E^2L
E^3L
E^4L
4EK_A
3EK_A/2
2EK_A/3
EK_A/4

Figure 5

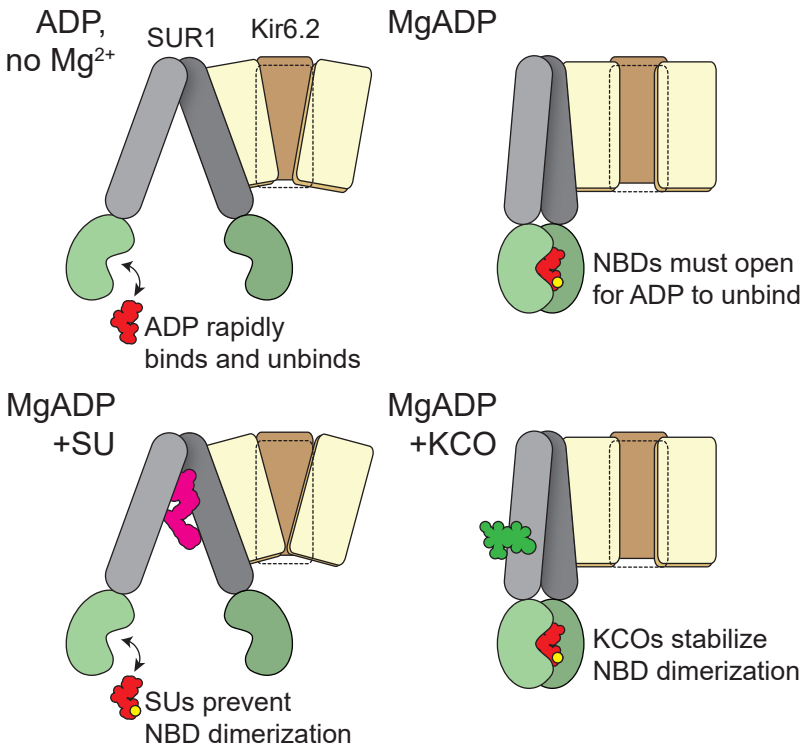
ADP,
no Mg2+
SUR1
Kir6.2
ADP rapidly
binds and unbinds
MgADP
NBDs must open
for ADP to unbind
MgADP
+SU
SUs prevent
NBD dimerization
MgADP
+KCO
KCOs stabilize
NBD dimerization

Figure 6

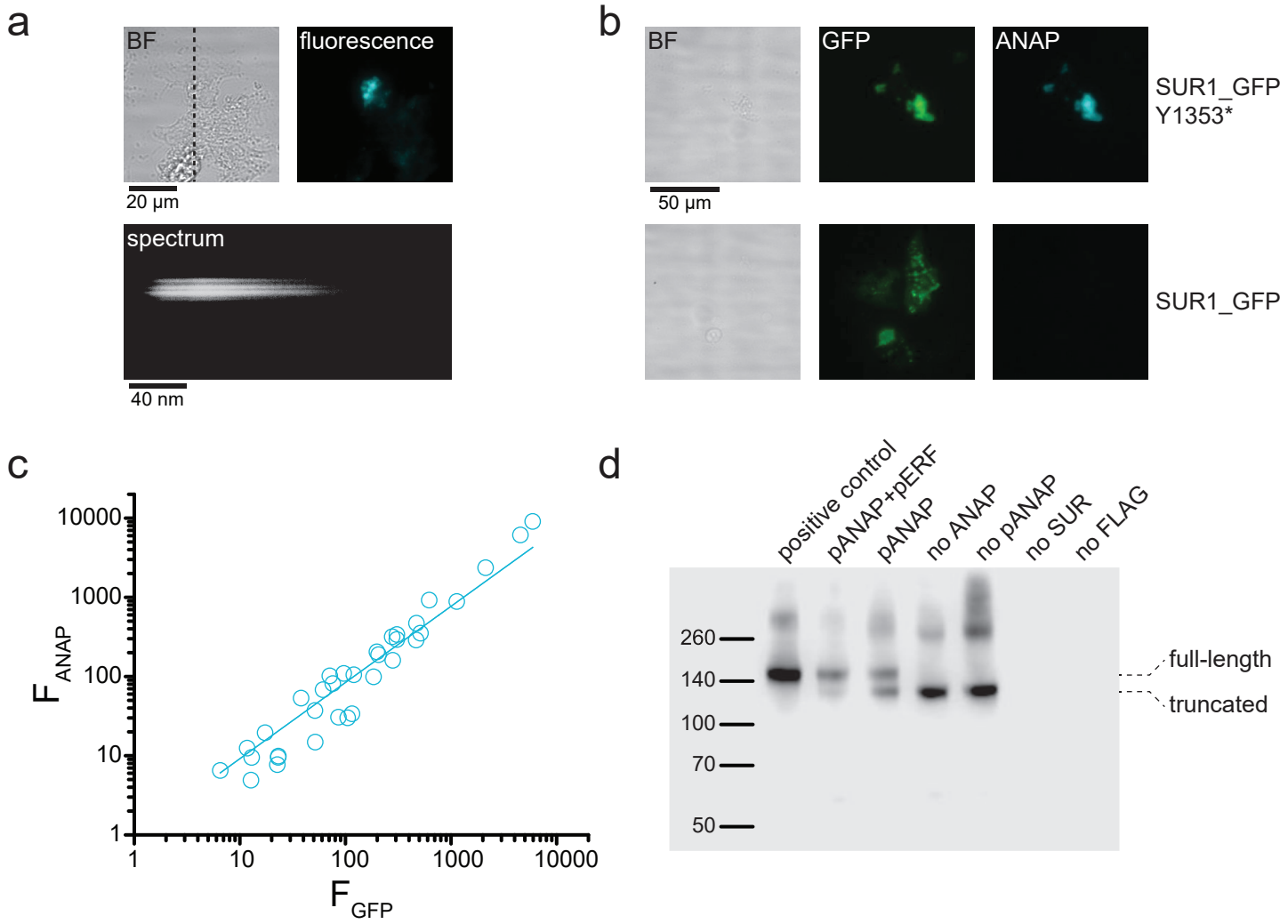
a
BF
fluorescence
20 µm
spectrum
40 nm
b
BF
GFP
ANAP
SUR1_GFP
Y1353*
50 µm
SUR1_GFP
c
10000
1000
100
10
1
F ANAP
1
10
100
1000
10000
F GFP
d
positive control
pANAP+pERF
pANAP
no ANAP
no pANAP
no SUR
no FLAG
260
140
100
70
50
full-length
truncated

Figure S1

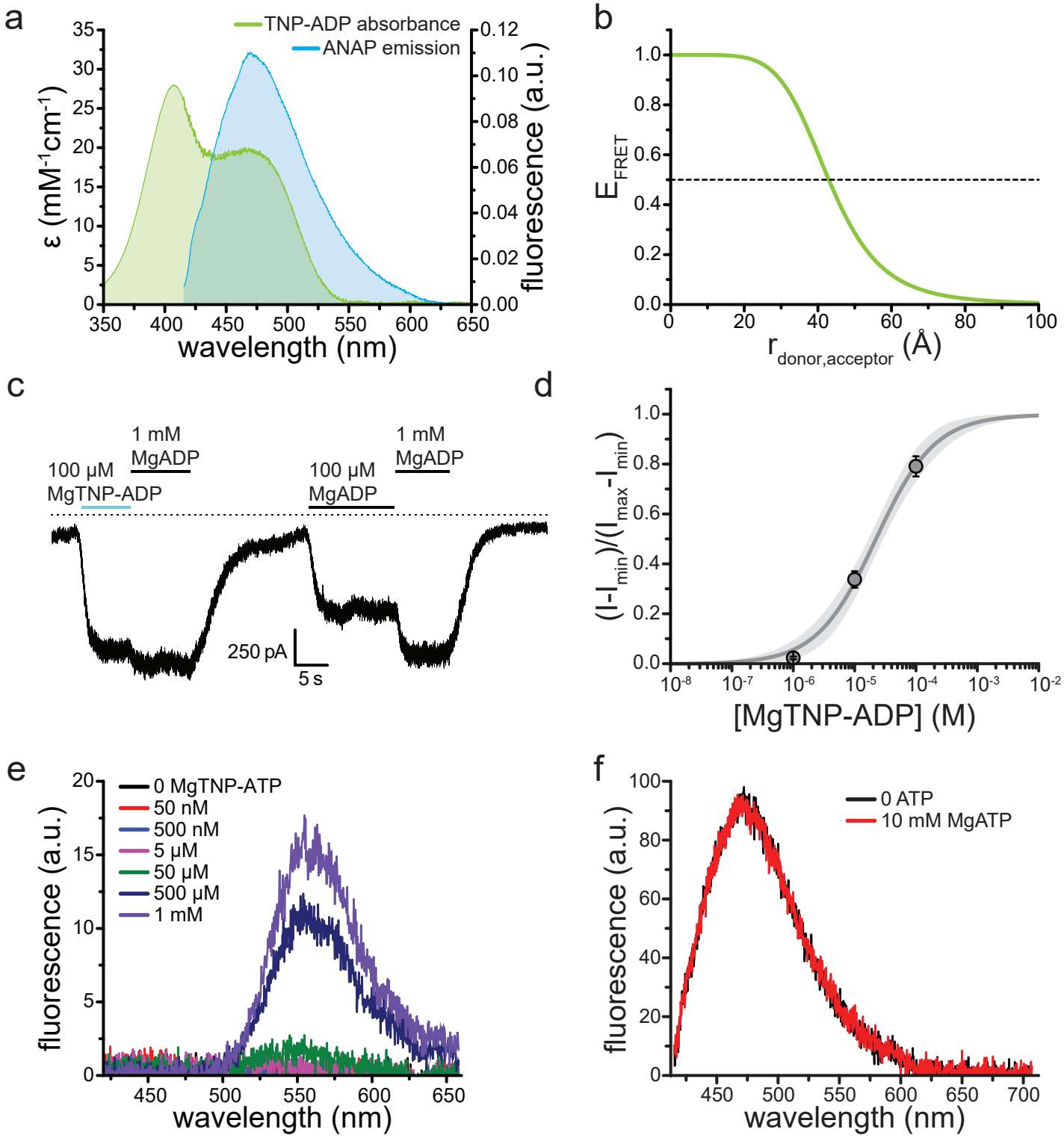
a
TNP-ADP absorbance
ANAP emission
ε (mM-1cm-1)
fluorescence (a.u.)
wavelength (nm)
b
EFRET
rdonor,acceptor (Å)
c
100 μM MgTNP-ADP
1 mM MgADP
100 μM MgADP
1 mM MgADP
250 pA
5 s
d
(I-Imin)/(Imax-Imin)
[MgTNP-ADP] (M)
e
0 MgTNP-ATP
50 nM
500 nM
5 μM
50 μM
500 μM
1 mM
fluorescence (a.u.)
wavelength (nm)
f
0 ATP
10 mM MgATP
fluorescence (a.u.)
wavelength (nm)

Figure S2

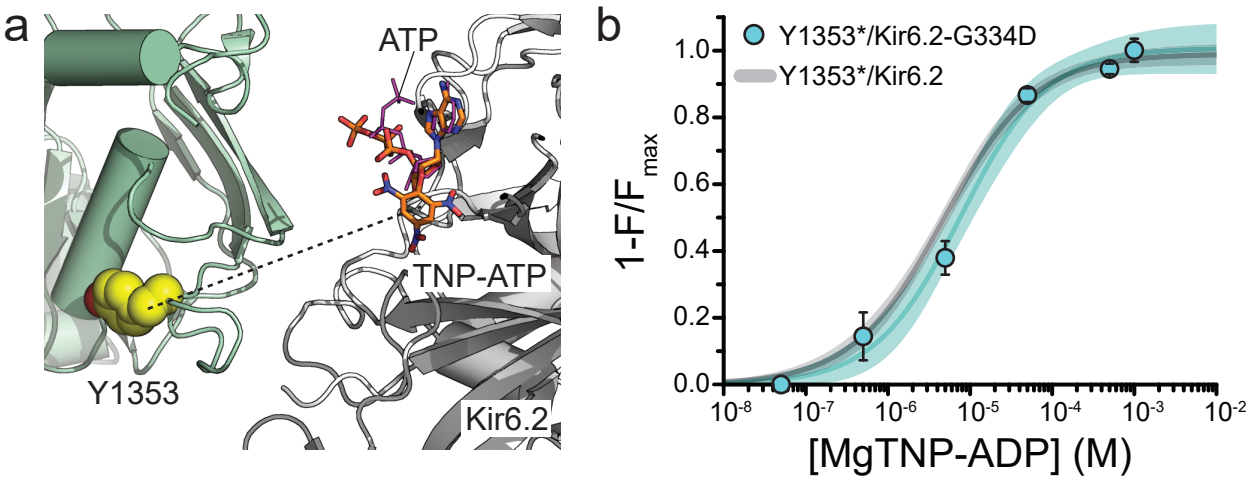
a
ATP
TNP-ATP
Y1353
Kir6.2
b
Y1353*/Kir6.2-G334D
Y1353*/Kir6.2
1-F/F max
1.0
0.8
0.6
0.4
0.2
0.0
10-8
10-7
10-6
10-5
10-4
10-3
10-2
[MgTNP-ADP] (M)

Figure S3

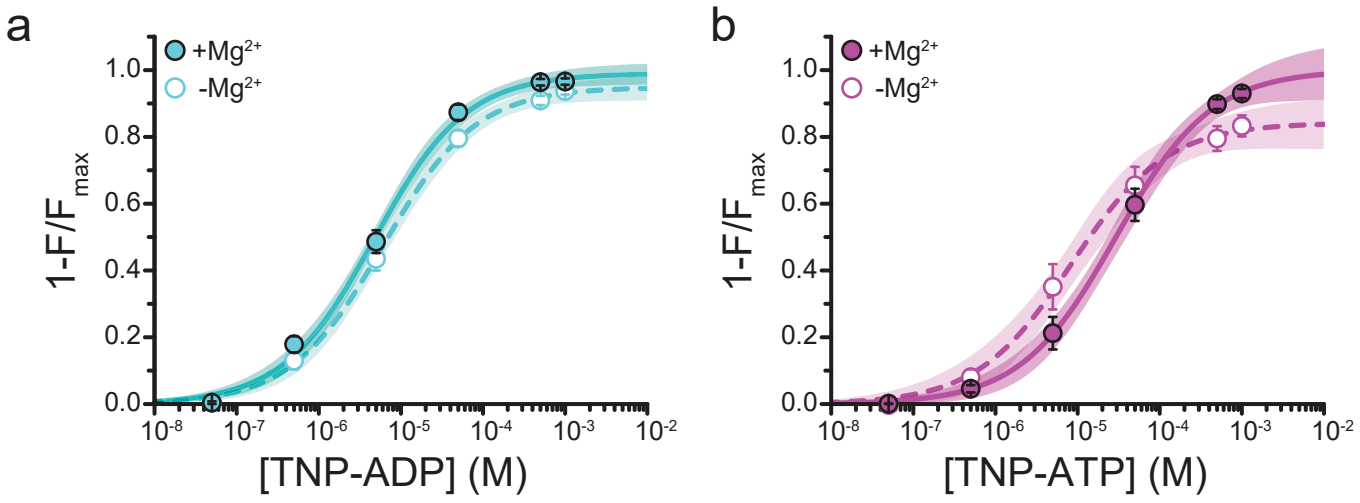
a
+Mg2+
-Mg2+
1-F/Fmax
1.0
0.8
0.6
0.4
0.2
0.0
10-8
10-7
10-6
10-5
10-4
10-3
10-2
[TNP-ADP] (M)
b
+Mg2+
-Mg2+
1-F/Fmax
1.0
0.8
0.6
0.4
0.2
0.0
10-8
10-7
10-6
10-5
10-4
10-3
10-2
[TNP-ATP] (M)

Figure S4

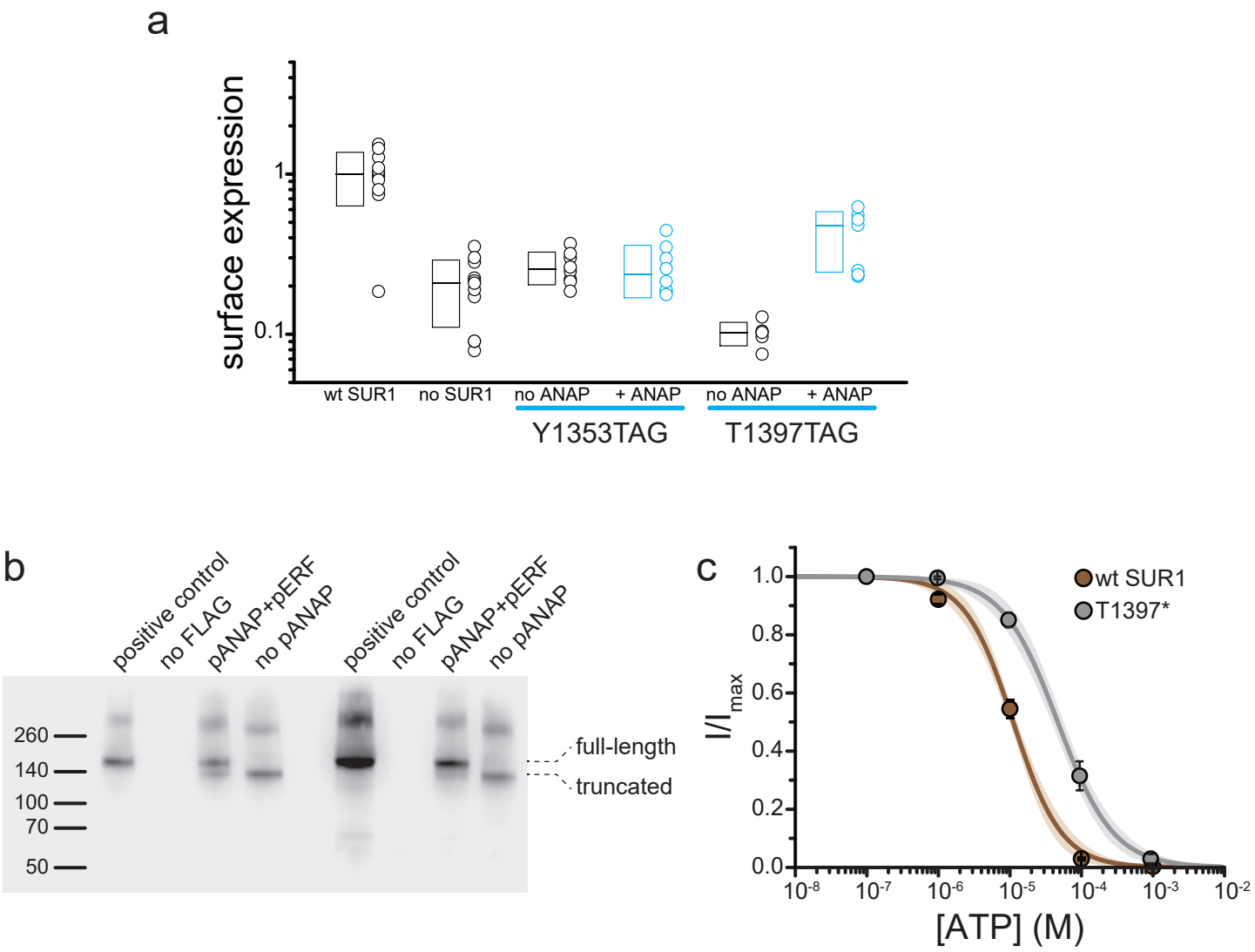
a
surface expression
1
0.1
wt SUR1
no SUR1
no ANAP
+ ANAP
no ANAP
+ ANAP
Y1353TAG
T1397TAG
b
positive control
no FLAG
pANAP+pERF
no pANAP
positive control
no FLAG
pANAP+pERF
no pANAP
260
140
100
70
50
full-length
truncated
c
wt SUR1
T1397*
I/I max
1.0
0.8
0.6
0.4
0.2
0.0
10-8
10-7
10-6
10-5
10-4
10-3
10-2
[ATP] (M)

Figure S5

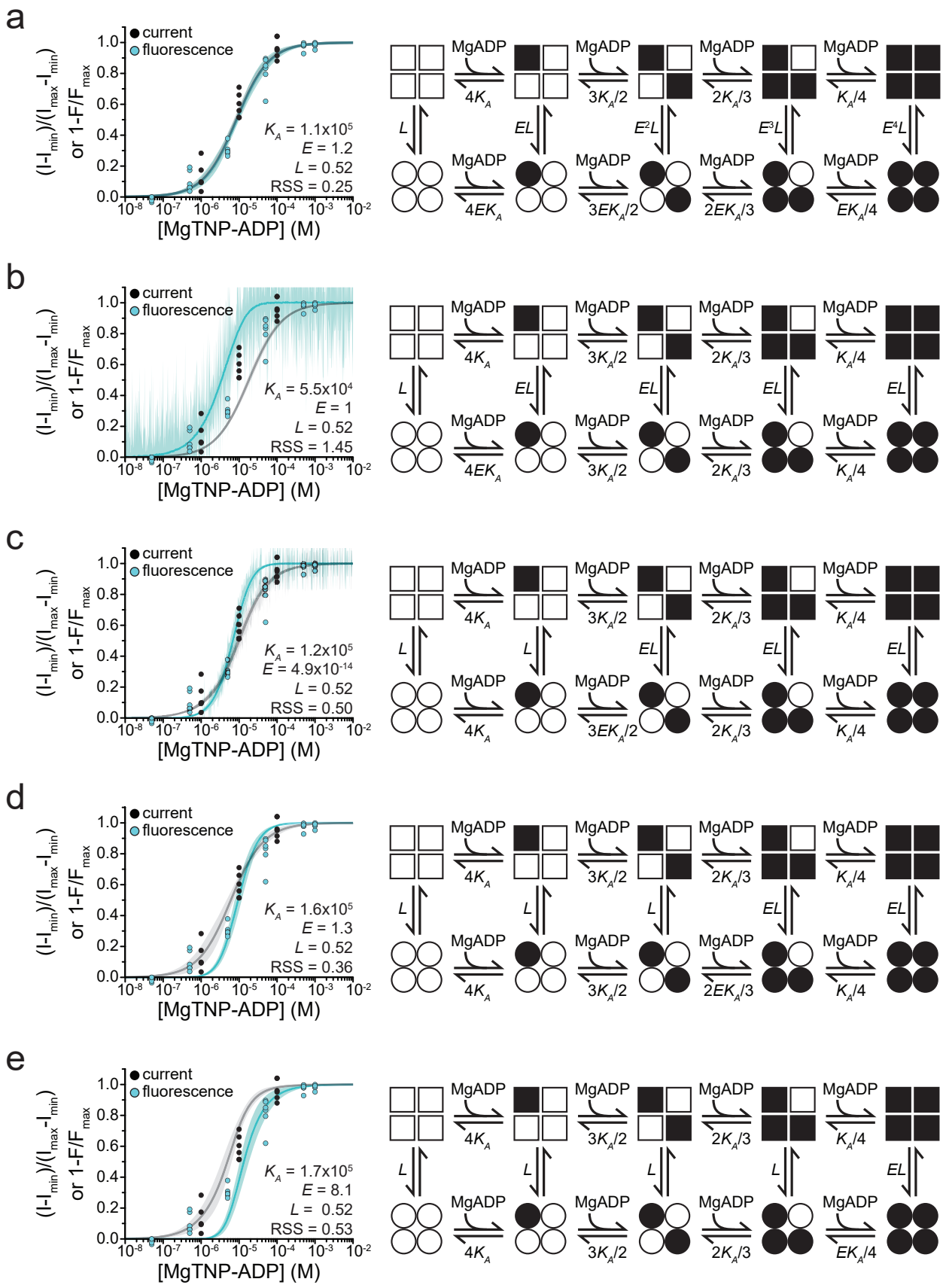
a
current
fluorescence
K_A = 1.1x10^5
E = 1.2
L = 0.52
RSS = 0.25
[MgTNP-ADP] (M)
b
K_A = 5.5x10^4
E = 1
L = 0.52
RSS = 1.45
c
K_A = 1.2x10^5
E = 4.9x10^-14
L = 0.52
RSS = 0.50
d
K_A = 1.6x10^5
E = 1.3
L = 0.52
RSS = 0.36
e
K_A = 1.7x10^5
E = 8.1
L = 0.52
RSS = 0.53
MgADP
L
EL
E^2L
E^3L
E^4L
$4K_A$
$3K_A/2$
$2K_A/3$
$K_A/4$
$4EK_A$
$3EK_A/2$
$2EK_A/3$
$EK_A/4$

Figure S6